

Conditional Extremes with Graphical Models

Aiden Farrell^{1,*}, Emma F. Eastoe^{1,†}, and Clement Lee^{2,‡}

¹*School of Mathematical Sciences, Fylde College, Lancaster University, UK*

²*School of Mathematics, Statistics and Physics, Herschel Building,
Newcastle University, UK*

Abstract

Multivariate extreme value analysis quantifies the probability and magnitude of joint extreme events. River discharges from the upper Danube River basin provide a challenging dataset for such analysis because the data, which is measured on a spatial network, exhibits both asymptotic dependence and asymptotic independence. To account for both features, we extend the conditional multivariate extreme value model (CMEVM) with a new approach for the residual distribution. This allows sparse (graphical) dependence structures and fully parametric prediction. Our approach fills a current gap in statistical methodology for graphical extremes, where existing models require asymptotic independence. Further, the model can be used to learn the graphical dependence structure when it is unknown *a priori*. To support inference in high dimensions, we propose a stepwise inference procedure that is computationally efficient and loses no information or predictive power. We show our method is flexible and accurately captures the extremal dependence for the upper Danube River basin discharges.

Keywords: Extremal dependence, graphical extremes, conditional multivariate extremes, sparsity, river networks

1 Introduction

The development of statistical models to describe and predict multivariate extreme events is an ongoing challenge in extreme value analysis. The field is also crucial in natural hazard

*a.farrell1@lancaster.ac.uk

†e.eastoe@lancaster.ac.uk

‡clement.lee@newcastle.ac.uk

risk assessment, especially for data arising from spatial, temporal, and spatio-temporal processes. For example, multivariate extreme value models have been adopted to predict risk from extreme snowfall (Blanchet and Davison, 2011), sea surface temperature (Simpson and Wadsworth, 2021), droughts (Oesting and Stein, 2018), river flows (Asadi et al., 2015; Keef et al., 2013), forest fires (Stephenson et al., 2015), precipitation (Westra and Sisson, 2011), wind-speed (Engelke et al., 2015), and ocean storms (Shooter et al., 2019), all of which exhibit complex behaviour, which can only be effectively captured by a flexible, multi-parameter model.

Multivariate extreme value models use the concept of extremal dependence. Consider a d -dimensional random vector $X = \{X_j : j \in V\}$ for $V = \{1, \dots, d\}$, with joint distribution function $F_X(x) = \mathbb{P}[X \leq x]$ and marginal distribution functions $F_j(x_j) = \mathbb{P}[X_j \leq x_j]$. Define the measure $\chi_A = \lim_{u \rightarrow 1} \mathbb{P}[F_i(X_i) > u : i \in A] / (1 - u)$ such that $A \subseteq V$ and $|A| \geq 2$ (Simpson et al., 2020). If $\chi_A > 0$, then the variables in A experience their extremes simultaneously and belong to the extremal dependence class of asymptotic dependence (AD). Full AD occurs when $\chi_A > 0$ for all $A \subseteq V$. If $\chi_A = 0$, then the variables in A cannot be simultaneously extreme. Furthermore, if $\chi_A = 0$ and $|A| = 2$, then the two variables belong to the extremal dependence class of asymptotic independence (AI) (Ledford and Tawn, 1996). Full AI occurs when $\chi_A = 0$ for all two-dimensional subsets of V . While independence implies AI, the converse is not true. The coefficient of tail dependence η (Ledford and Tawn, 1996) identifies pairs of variables that exhibit AI as either exactly independent ($\eta = 0.5$) or negatively ($0 < \eta < 0.5$) or positively ($0.5 < \eta < 1$) associated.

We consider river discharges in the upper Danube River basin. Daily discharge data at $d = 31$ gauging stations for 1960-2009 is available from the Bavarian Environmental Agency (<http://www.gkd.bayern.de>). Figure 1 (left panel) shows the undirected tree implied by the flow connections of the river basin. We use the summer-only, temporally declustered dataset (see Asadi et al. (2015) for details), made available in the `graphicalExtremes` package (Engelke et al., 2024b) in R (R Core Team, 2024). The data have previously been analysed using a max-stable Brown Resnick process (Asadi et al., 2015) and a multivariate Pareto graphical model (Engelke and Hitz, 2020), both of which assume full AD. Figure 1 (right panel) shows scatter plots on standard Fréchet margins, and empirical estimates for the extremal dependence measures $\bar{\chi}(u)$ and $\chi(u)$ (Coles et al., 1999) for stations 19 and 29 (top), and 19 and 16 (bottom). The former pair lie on different tributaries and are flow-unconnected, while the latter pair lie on the Isar tributary and are flow-connected. Stations 19 and 16 appear to experience extreme events simultaneously, supported by the fact that $\bar{\chi}(u) \rightarrow 1$ as $u \rightarrow 1$, and exhibit AD. Conversely, the scatter plots for stations 19 and 29 suggest they exhibit AI, which is supported by the fact that $\bar{\chi}(u) \not\rightarrow 1$ as $u \rightarrow 1$. Thus,

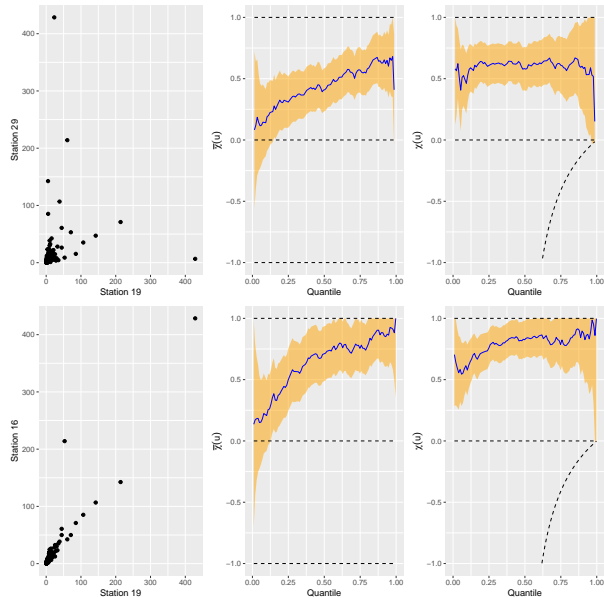
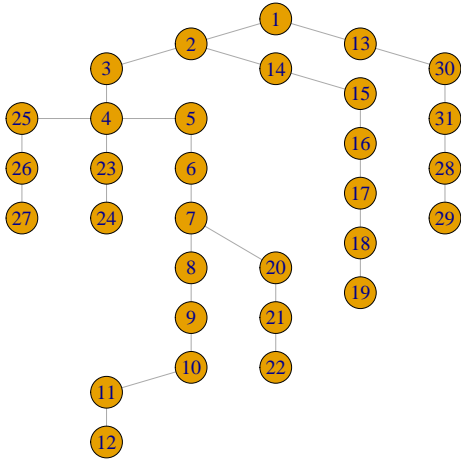


Figure 1: Undirected tree induced by the flow connections of the upper Danube River basin (left). Exploratory data analysis (right) of the extremal dependence between stations 19 and 29 (top) and 19 and 16 (bottom). The panels display scatter plots of the declustered discharges on standard Fréchet margins (left), and empirical estimates, including 95% confidence intervals, of $\bar{\chi}(u)$ (centre), $\chi(u)$ (right) for $u \in [0, 1]$.

while flow-connected stations often experience extreme events simultaneously, some flow-unconnected stations do not. Assuming AD for such stations leads to an overestimation of their joint tail behaviour. This motivates the need for a model that can capture both AD and AI while also incorporating flow connectivity.

Returning to multivariate extreme value models, we observe that there is a rich set of models based on max-stable distributions and processes. Examples include the multivariate Pareto distribution (Rootzén and Tajvidi, 2006; Rootzén et al., 2018), and the max-stable (Smith, 1990) and generalised r -Pareto (Ferreira and de Haan, 2014) processes. The process formulations form the basis of spatial (de Fondeville and Davison, 2018; Reich and Shaby, 2012; Ribatet, 2013), temporal (Schlather, 2002; Smith et al., 1997), and spatio-temporal (Davis et al., 2013; Huser and Davison, 2014; Opitz et al., 2018) models for extremes, and the multivariate Pareto distribution forms the basis for the existing graphical modelling approach for extremes (Engelke et al., 2024a). Such models appeal due to their links to asymptotic limit theory; however, the underlying multivariate distribution must be in the domain of attraction of a max-stable distribution and therefore have full AD (de Haan and Resnick, 1987), rendering them unsuitable for many datasets, including the Danube discharges.

AI models, such as the one proposed by Ledford and Tawn (1997), were initially limited

to the bivariate case only. While Ramos and Ledford (2011) and Wadsworth and Tawn (2013) developed extensions of this model that allowed for inference away from the diagonal, the semi-parametric conditional multivariate extreme value model (CMEVM) was the first model to provide a credible approach to data exhibiting both AI and AD (Heffernan and Tawn, 2004). The CMEVM is not based on a multivariate distribution or process; rather, conditional on one variable being large, normalising functions are defined to control the rate of growth of all other variables such that, after normalisation, the joint distribution of these “residuals” is non-degenerate. The model has gained popularity due to the relative ease with which its parameters can be estimated and interpreted, even in high dimensions. Applications include flood risk mapping (Neal et al., 2013; Towe et al., 2019), and the prediction of extreme sea states (Gouldby et al., 2014, 2017; Ross et al., 2020), sea surface temperatures (Simpson and Wadsworth, 2021), heatwaves (Winter and Tawn, 2016), and precipitation (Debushe and Diriba, 2021; Richards et al., 2022).

However, the predictive performance of the CMEVM declines with increasing dimensionality due to a non-parametric component. The recent spatial CMEVM (Richards et al., 2022; Shooter et al., 2021; Wadsworth and Tawn, 2022) overcomes this by using a fully parametric spatial kernel for the residual distribution. By construction, this spatial model is appropriate for measurements on a continuous spatial surface but not for measurements on alternative topographies, such as road or river networks, which are represented by a graphical structure, such as that in Figure 1. Meanwhile, Casey and Papastathopoulos (2023) have developed a theoretical framework for the CMEVM for processes observed on a chordal graph with singleton separator sets, but they have not developed this into a statistical model.

Our contribution fills these gaps. We present the multivariate asymmetric generalised Gaussian (MVAGG) to model the CMEVM residuals, thus enabling fully parametric prediction. Inference in high dimensions is achieved using stepwise optimisation procedures that are computationally efficient, without any loss of information or predictive performance. Our model can also incorporate structure into the CMEVM residuals, thereby providing a framework for graphical structures that accommodates both extremal dependence classes. Our model generalises the temporal Markov model for extremes of Winter and Tawn (2017), but to the best of our knowledge, is the first model to incorporate a general graphical structure in the CMEVM.

The remainder of this paper is structured as follows. Section 2 provides an overview of the CMEVM, introduces the MVAGG distribution, and describes the proposed structured CMEVM. Model inference, graphical selection, and model-based predictions are provided in Section 3. In Section 4, we illustrate the performance of our model and the graphical

selection procedure, as well as the utility of the stepwise inference procedures. We then apply our model to river discharges in the upper Danube River basin (Asadi et al., 2015) in Section 5, and compare our model to the one proposed by Engelke and Hitz (2020). Finally, we outline directions for future research in Section 6.

2 Methodology

We review the CMEVM, the MVAGG distribution and graphical models, before combining these to form a variant of the CMEVM that incorporates graphical structures into the residual distribution. For notation: let $V_{|i} = V \setminus \{i\}$ and $X_{|i}$ denote the set V excluding element i and the vector $\{X_j : j \in V_{|i}\}$, respectively.

2.1 Conditional Multivariate Extreme Value Model

For mathematical convenience, we define the CMEVM on standard Laplace margins Keef et al. (2013); this is not restrictive as the PIT can be used to transform arbitrary margins to this scale without altering the dependence structure Sklar (1959). Let Y and $Y_{|i}$ denote X and $X_{|i}$ following this transformation. Next, assume there exists normalising functions $\{a_{j|i} : \mathbb{R} \rightarrow \mathbb{R}, j \in V_{|i}\}$ and $\{b_{j|i} : \mathbb{R} \rightarrow \mathbb{R}_+, j \in V_{|i}\}$, such that for any $i \in V$,

$$\left(\left\{ \frac{Y_j - a_{j|i}(Y_i)}{b_{j|i}(Y_i)} \right\}_{j \in V_{|i}}, Y_i - u_{Y_i} \right) \Big| Y_i > u_{Y_i} \xrightarrow{d} (\{Z_{j|i} : j \in V_{|i}\}, E), \quad (2.1)$$

as $u_{Y_i} \rightarrow \infty$. In the limit, the residual vector $Z_{|i} = \{Z_{j|i} : j \in V_{|i}\}$ is independent of Y_i and has a non-degenerate distribution, while the limit variable E follows a standard exponential distribution Heffernan and Resnick (2007). Consequently, inference can be split into inference on: (i) $Y_i | Y_i > u_{Y_i}$; (ii) the normalising functions; and (iii) $Z_{|i}$. The first is trivial, since the tail of $Y_i | Y_i > u_{Y_i}$ is standard exponential by limit (2.1). Parts (ii) and (iii) require consideration. For the normalising functions, Heffernan and Tawn (2004) propose the form

$$a_{j|i}(y_i) = \alpha_{j|i} y_i, \quad b_{j|i}(y_i) = y_i^{\beta_{j|i}}$$

where $\alpha_{j|i} \in [1, 1]$ and $\beta_{j|i} \in (-\infty, 1]$. These flexible functions capture AD ($\alpha_{j|i} = 1$ and $\beta_{j|i} = 0$), complete independence ($\alpha_{j|i} = 0$), and AI (all other parameter combinations). Further, the pairwise formulation can identify dependence structures in which some pairs of variables exhibit AD while others exhibit AI, without prior specification of this structure.

Unlike the normalising functions, there is no general class of distributions to model the residuals $Z_{|i}$. Heffernan and Tawn (2004) use the working assumption that $Z_{|i}$ follows a $(d - 1)$ -dimensional multivariate Gaussian (MVG) distribution, denoted $Z_{|i} \sim \text{MVG}_{d-1}(\boldsymbol{\mu}_{|i}, \Sigma_{|i}^*)$, with mean vector $\boldsymbol{\mu}_{|i} = \{\mu_{j|i} : j \in V_{|i}\} \in \mathbb{R}^{d-1}$, and symmetric, positive-definite *covariance* matrix $\Sigma_{|i}^*$. To further simplify they assume independence between the components of $Z_{|i}$ i.e., $\Sigma_{|i}^*$ is a diagonal matrix. Given n independent realisations $\{y^1, \dots, y^n\}$ of the random vector Y , they perform inference for each component Y_i separately by maximising the likelihood

$$L_{|i}(\boldsymbol{\theta}_{|i}) = \prod_{k: y_i^k > u_{Y_i}} \phi_{d-1} \left[\left\{ \frac{y_j^k - \alpha_{j|i} y_i^k}{(y_i^k)^{\beta_{j|i}}} \right\}_{j \in V_{|i}} ; \boldsymbol{\mu}_{|i}, \Sigma_{|i}^* \right] \prod_{j \in V_{|i}} (y_i^k)^{-\beta_{j|i}}, \quad (2.2)$$

where $\phi_{d-1}(\cdot; \boldsymbol{\mu}_{|i}, \Sigma_{|i}^*)$ is the density of the $(d - 1)$ -dimensional MVG distribution. To avoid over-reliance on the working assumptions, their prediction is semi-parametric; the residuals are sampled with replacement from the fitted residuals

$$\hat{z}_{|i} = \{\hat{z}_{j|i} := (y_{j|i} - \hat{\alpha}_{j|i} y_i) y_i^{-\hat{\beta}_{j|i}} : j \in V_{|i}\}, \quad (2.3)$$

where hat notation denotes maximum likelihood estimates of parameters, before being back-transformed onto the original scale. However, the approach does not scale well with dimension (see Supplementary Material Farrell et al. (2024)) as sampling from the empirical distribution suffers from the curse of dimensionality Nagler and Czado (2016).

2.2 Multivariate Asymmetric Generalised Gaussian Distribution

By assuming a flexible distribution for the residuals $Z_{|i}$, we propose a fully parametric extension of the CMEVM. Using a similar approach to the spatial CMEVM Richards et al. (2022); Shooter et al. (2021), we define the margins and dependence structure of the distribution separately. For the margins, we choose an asymmetric generalised Gaussian (AGG) distribution Nacereddine and Goumeidane (2019) with density

$$f_Z(z) = \frac{\delta}{(\kappa_1 + \kappa_2)\Gamma(1/\delta)} \begin{cases} \exp\left\{-[(\nu - z)/\kappa_1]^\delta\right\} & \text{for } z < \nu \\ \exp\left\{-[(z - \nu)/\kappa_2]^\delta\right\} & \text{for } z \geq \nu, \end{cases} \quad (2.4)$$

where $z \in \mathbb{R}$, $\Gamma(\cdot)$ denotes the standard gamma function, and $\nu \in \mathbb{R}$, $\kappa_1 > 0$, $\kappa_2 > 0$, $\delta > 0$ are the location, left-scale, right-scale, and shape parameters, respectively. We refer to this distribution as the $\text{AGG}(\nu, \kappa_1, \kappa_2, \delta)$. When $\kappa_1 = \kappa_2$, the AGG reduces to the generalised

Gaussian (or delta-Laplace) distribution used in the spatial CMEVM to bridge the Gaussian ($\delta = 2$) and Laplace ($\delta = 1$) distributions i.e., the anticipated residual marginal distributions under AD and exact independence respectively Wadsworth and Tawn (2022).

We next assume that the residuals, following transformation from AGG to standard Gaussian margins, follow a MVG distribution. Formally, if $W_{j|i} = \Phi^{-1}(F_{Z_{j|i}}(Z_{j|i}))$, where Φ and $F_{Z_{j|i}}$ are the distribution functions of the standard Gaussian and AGG distributions, respectively, then $W_{|i} = \{W_{j|i} : j \in V_{|i}\} \sim \text{MVG}_{d-1}(\mathbf{0}, \Sigma_{|i})$ for a $(d-1)$ -dimensional symmetric, positive-definite *correlation* matrix $\Sigma_{|i}$. We call the combination of marginal and joint distributions the multivariate asymmetric generalised Gaussian (MVAGG) distribution and denote this by $Z_{|i} \sim \text{MVAGG}_{d-1}(\Theta_{|i}, \Theta_{|i}^\Gamma)$, where $\Theta_{|i} := \{(\nu_{j|i}, \kappa_{2j|i}, \kappa_{1j|i}, \delta_{j|i}) : j \in V_{|i}\}$ and $\Theta_{|i}^\Gamma$ contains the parameters that populate the (sparse) precision matrix $\Gamma_{|i} := (\Sigma_{|i})^{-1}$. The density for this distribution is

$$f_i(z_{|i}) = \phi_{d-1} \left[\left\{ \Phi^{-1} \left(F_{Z_{j|i}}(z_{j|i}) \right) \right\}_{j \in V_{|i}} ; \mathbf{0}, \Sigma_{|i} \right] \prod_{j \in V_{|i}} \frac{f_{Z_{j|i}}(z_{j|i})}{\phi \left[\Phi^{-1} \left(F_{Z_{j|i}}(z_{j|i}) \right) \right]} \quad (2.5)$$

where $f_{Z_{j|i}}$ is defined in equation (2.4), and ϕ is the standard univariate Gaussian density.

2.3 Structured Conditional Multivariate Extreme Value Model

While the MVAGG CMEVM overcomes the curse of dimensionality, the correlation matrix $\Sigma_{|i}$ increases the number of parameters to order d^3 . This is much greater than both the original CMEVM and the spatial CMEVM, and is computationally prohibitive for large d . We therefore propose a graphical model for the Gaussian copula of the MVAGG. A simple undirected graph $\mathcal{G} = (V, E)$ consists of a vertex set $V = \{1, \dots, d\}$ and edge set $E \subseteq \{\{j, k\} \mid j, k \in V, j \neq k\}$ with $\{j, k\} \in E$ if and only if $\{k, j\} \in E$. For a random variable $W \sim \text{MVG}_d(\mathbf{0}, \Sigma)$, with precision matrix $\Gamma = (\Sigma)^{-1}$, if $\{j, k\} \notin E$, then W_j and W_k are conditionally independent given the remaining components. For the Gaussian distribution, this corresponds to the partial correlation of W_j and W_k being zero which, in turn, implies that $\Gamma_{j,k} = \Gamma_{k,j} = 0$ Speed and Kiiveri (1986). Thus a sparse precision matrix (equivalently \mathcal{G}) may greatly reduce the dimension of the parameter space.

We now introduce the MVAGG structured CMEVM (MVAGG SCMEVM). The CMEVM part of the model requires that a (conditional) distribution is specified for the $(d-1)$ -dimensional residual vector $Z_{|i}$ for each $i \in V$. Using the copula construction of the MVAGG, we have $W_{|i} \sim \text{MVG}_{d-1}(\mathbf{0}, \Sigma_{|i})$. Rather than defining a separate graphical structure for each

conditioning component, we instead infer them from the graph \mathcal{G} for the d -dimensional vector W , where W is constructed by augmenting $W_{\setminus i}$ with an i th element $W_i = 0$. Exploiting properties of the conditional Gaussian distribution, the structure of $\Gamma_{\setminus i}$ is the same as for Γ but excluding the i th row and column. Equivalently, $W_{\setminus i}$ has graph $\mathcal{G}_{\setminus i}$ formed by removing the i th node and its incident edges from \mathcal{G} . Inclusion of $W_i = 0$ follows by including the degenerate normalising function $a_{i|i}(y) = y$ in the first step of the CMEVM, thus augmenting the residual vector $Z_{\setminus i}$ by the component $Z_i = 0$. The constraint that $W_i = 0$ follows if $Z_i \sim \text{AGG}(0, 1, 1, 1)$. Lastly, we note that while a more flexible copula, such as an elliptical distribution or an extreme value copula, might be used instead of the Gaussian copula, conditional independence does not result in analogous simplifications.

3 Inference

We describe an efficient inference procedure for the MVAGG SCMEVM and provide algorithms for graphical selection and model-based predictions.

3.1 Parameter estimation

Given n independent and identically distributed realisations $\{x^1, \dots, x^n\}$ of the d -dimensional random vector X , the first step is transformation to standard Laplace margins. By double application of the PIT, for each $i \in V$ and each $k \in \{1, \dots, n\}$,

$$y_i^k = \begin{cases} -\log \left(2 \left[1 - \tilde{F}_i(x_i^k) \right] \right) & \tilde{F}_i(x_i^k) > 0.5, \\ \log \left(2\tilde{F}_i(x_i^k) \right) & \tilde{F}_i(x_i^k) \leq 0.5, \end{cases}$$

where \tilde{F}_i is an estimate of the marginal distribution F_i for X_i . We use a semi-parametric estimate for F_i consisting of the empirical distribution for $x_i \leq v_{X_i}$ and a generalised Pareto distribution for $x_i > v_{X_i}$ (Heffernan and Tawn, 2004). The threshold v_{X_i} is selected using the automated method of Murphy et al. (2024).

Inference for the MVAGG SCMEVM is performed for each component Y_i separately by maximising the likelihood

$$L_{\setminus i}(\boldsymbol{\theta}_{\setminus i}) = \prod_{k: y_i^k > u_{Y_i}} f_i \left(\left\{ \frac{y_j^k - \alpha_{j|i} y_i^k}{(y_i^k)^{\beta_{j|i}}} \right\}_{j \in V_{\setminus i}} ; \boldsymbol{\Theta}_{\setminus i}, \boldsymbol{\Theta}_{\setminus i}^{\Gamma} \right) \prod_{j \in V_{\setminus i}} (y_i^k)^{-\beta_{j|i}}, \quad (3.1)$$

where f_i is given by equation (2.5), u_{Y_i} is the dependence threshold and $\boldsymbol{\theta}_{|i} := (\boldsymbol{\Theta}_{|i}^d, \boldsymbol{\Theta}_{|i}, \boldsymbol{\Theta}_{|i}^\Gamma)$ combines the CMEVM dependence $\boldsymbol{\Theta}_{|i}^d := \{(\alpha_{j|i}, \beta_{j|i}) : j \in V_{|i}\}$, MVAGG marginal $\boldsymbol{\Theta}_{|i}$ and MVAGG correlation $\boldsymbol{\Theta}_{|i}^\Gamma$ parameters. Algorithm 3.1 gives an iterative numerical maximisation procedure. Treating $\boldsymbol{\Theta}_{|i}^d$ and $\boldsymbol{\Theta}_{|i}$ as fixed in step 3 of the algorithm, inference reduces to maximising the profile log-likelihood of a $\text{MVG}_{d-1}(\mathbf{0}, \Sigma_{|i})$ distribution. An analytical expression for $\hat{\Gamma}_{|i} = (\hat{\Sigma}_{|i})^{-1}$ is available if the residuals are either independent (trivially) or have saturated covariance structure. For the latter, $\hat{\Gamma}_{|i}$ is the inverse of the empirical correlation matrix of the transformed vector $\hat{w}_{|i}$ where $\hat{w}_{j|i} = \Phi^{-1}(F_{Z_{j|i}}(\hat{z}_{j|i}; \hat{\boldsymbol{\Theta}}_{j|i}))$. Numerical optimisation is required when incorporating a graphical structure \mathcal{G} with the graphical lasso (Friedman et al., 2007, 2019) used to penalise elements for which edges do not exist in \mathcal{G} , ensuring that the corresponding entries in $\hat{\Gamma}_{|i}$ are 0.

This procedure has limitations. Firstly, the parameter space cannot be easily constrained to ensure that the first-order extremal dependence structure is captured by $\boldsymbol{\Theta}_{|i}^d$ and not the residual distribution. Secondly, even for a sparse precision matrix $\Gamma_{|i}$, the number of parameters to jointly maximise grows at least linearly in d , and finding suitable starting values for the optimisation becomes difficult for large d . We therefore prefer the two- and three-step procedures described in Algorithm 3.2. Both approaches combat the first limitation. However, the two-step approach still requires a second high-dimensional, computationally expensive, numerical optimisation procedure (Algorithm 3.3). The three-step approach circumvents this and is therefore our preference. Lastly, we observe that there is no information gained by jointly fitting the d conditional models since the parameter values in the MVAGG may differ with each conditioning variable; this is in contrast to the spatial CMEVM (Richards et al., 2022; Wadsworth and Tawn, 2022) which has a stationary residual spatial process and hence the parameters do not change with the conditioning site.

3.2 Graph selection

The graphical structure may not be known *a priori*. Therefore, we require a method to determine the optimal graphical structure \mathcal{G} . Recall that \mathcal{G} is defined for the augmented vector W , not $W_{|i}$. Consequently, we could learn the graph for W using a composite likelihood. This would ensure consistency but would require multiple likelihood ratio tests and reduce the power of the test. Alternatively, we could iteratively add edges to \mathcal{G} that minimise the AIC (Engelke and Hitz, 2020). However, this is computationally expensive when d is large.

Our approach, detailed in Algorithm 3.4, uses the graphical lasso (Friedman et al., 2007) to learn the graphical structure of $W_{|i}$, for each $i \in V$. Since this need not result in consistent graphical structures, the d subgraphs are combined into a weighted graph \mathcal{G}^* and a majority

Algorithm 3.1 One-step parameter estimation for the MVAGG SCMEVM

- 1: Initialise $\Theta_{|i}^d$, $\Theta_{|i}$, and tol ;
 - 2: The current values of $\Theta_{|i}^d$ and $\Theta_{|i}$ are $\Theta_{|i}^{d*}$ and $\Theta_{|i}^*$, respectively.
 - 3: Obtain $\hat{\Theta}_{|i}^\Gamma = \underset{\Theta_{|i}^\Gamma}{\operatorname{argmax}} L_{|i} \left(\Theta_{|i}^{d*}, \Theta_{|i}^*, \Theta_{|i}^\Gamma \right)$, where $L_{|i}$ is likelihood (3.1);
 - 4: Obtain $\left(\hat{\Theta}_{|i}^d, \hat{\Theta}_{|i} \right) = \underset{\Theta_{|i}^d, \Theta_{|i}}{\operatorname{argmax}} L_{|i} \left(\Theta_{|i}^d, \Theta_{|i}, \hat{\Theta}_{|i}^\Gamma \right)$;
 - 5: **if** $\max(|\hat{\Theta}_{|i}^d - \Theta_{|i}^{d*}|, |\hat{\Theta}_{|i} - \Theta_{|i}^*|) > \text{tol}$ **then**
 - 6: Set $\Theta_{|i}^d = \hat{\Theta}_{|i}^d$ and $\Theta_{|i} = \hat{\Theta}_{|i}$
 - 7: Repeat 2. - 4.;
 - 8: **else**
 - 9: **return** $\hat{\Theta}_{|i}^d$, $\hat{\Theta}_{|i}$ and $\hat{\Theta}_{|i}^\Gamma$
 - 10: **end if**
-

rule is used to determine the best overall graph $\hat{\mathcal{G}}$. The approach has two tuning parameters: the CMEVM dependence threshold, and the graphical lasso penalisation parameter. The former can be checked with diagnostics discussed in Southworth et al. (2024). For the graphical lasso, we implement the procedure for several feasible values and select the final graph using another majority rule.

3.3 Prediction

By construction, the CMEVM does not have closed forms for either tail probabilities or quantiles. Heffernan and Tawn (2004) use a simulation-based prediction algorithm which samples from the empirical distribution of the fitted residuals $\hat{Z}_{|i}$. The model proposed in Section 2 allows for fully parametric predictions using a method that is very similar to that used by Wadsworth and Tawn (2022, Section 5.2.2) and Richards et al. (2022, Section 3.3).

We first note that the model describes

$$\left\{ F_{X_i}^{-1}(F_L(Y_i)) : i \in V \right\} \left| \left(\max_{i \in V} Y_i > u \right), \quad (3.2)$$

such that $u > \max(u_{Y_i} : i \in V)$ where u_{Y_i} is the dependence threshold used to fit our model in Section 3.1, and F_L denotes the distribution function of the standard Laplace distribution. To create realisations of X , we draw samples from equation (3.2) using Algorithm 3.5 with probability

$$\mathbb{P} \left(\max_{i \in V} Y_i > u \right) = \frac{1}{n} \sum_{k=1}^n \mathbb{1} \left\{ \max_{i \in V} y_i^k > u \right\}. \quad (3.3)$$

Algorithm 3.2 Stepwise parameter estimation for the MAVGG SCMEVM

- 1: Set **Steps** to be 2 or 3;
 - 2: Assuming independent Gaussian residuals, obtain $\hat{\Theta}_{|i}^d$ by maximising likelihood (2.2);
 - 3: Using equation (2.3) and $\hat{\Theta}_{|i}^d$, obtain $\hat{z}_{|i}$ and treat them as fixed;
 - 4: **if Steps==2 then**
 - 5: Use Algorithm 3.3 to obtain $\hat{\Theta}_{|i}$ and $\hat{\Theta}_{|i}^\Gamma$;
 - 6: **else if Steps==3 then**
 - 7: Assuming that the components of $\hat{Z}_{|i}$ are independent, obtain $\hat{\Theta}_{|i} = \operatorname{argmax}_{\Theta_{|i}} f_i(\hat{z}_{|i}; \Theta_{|i}, I_{d-1})$ where f_i is given by equation (2.5), and I_{d-1} is a $(d-1)$ -dimensional identity matrix;
 - 8: Obtain $\hat{\Theta}_{|i}^\Gamma = \operatorname{argmax}_{\Theta_{|i}^\Gamma} L_{|i}(\hat{\Theta}_{|i}^d, \hat{\Theta}_{|i}, \Theta_{|i}^\Gamma)$, where $L_{|i}$ is likelihood (3.1).
 - 9: **end if**
 - 10: **return** $\hat{\Theta}_{|i}^d$, $\hat{\Theta}_{|i}$ and $\hat{\Theta}_{|i}^\Gamma$
-

Otherwise, we draw realisations from the empirical distribution of $X \mid \left(\max_{i \in V} Y_i < u \right)$.

4 Simulation Study

We use simulation studies to assess the performance of the SCMEVM. The stepwise inference procedures are investigated in Section 4.1 and the graphical selection process is assessed in Section 4.2. Section 4.3 compares the SCMEVM to existing methods.

4.1 Stepwise inference procedures

Using data simulated from the SCMEVM with a graphical covariance structure, we compare parameter estimation for the one-, two-, and three-step procedures with independent, graphical and saturated covariance structures. We use the graph $\mathcal{G} = (V, E)$, $V = \{1, \dots, 5\}$ and $E = \{\{1, 2\}, \{1, 3\}, \{2, 3\}, \{3, 4\}, \{3, 5\}, \{4, 5\}\}$. For each $i \in V$, we simulate the conditioning variable $Y_i \mid Y_i > u_{Y_i}$ from a standard Laplace distribution with $u_{Y_i} = -\log(0.4)$ (the 0.80-quantile of this distribution). We obtain $Z_{|i}$ from a MVAGG distribution by (i) simulating $W_{|i}$ from a MVG distribution with standard Gaussian margins and correlation matrix $\Sigma_{|i}$ and (ii) transforming $W_{|i}$ onto AGG margins via the PIT. Using limit (2.1), we obtain $Y_{|i}$, and thereby a full d -dimensional vector for $Y \mid Y_i > u_{Y_i}$. We generate 200 samples of $Y \mid Y_i > u_{Y_i}$ and consider $n \in \{250, 500\}$. The true dependence and AGG parameters are independently sampled from a uniform distribution on $(0.1, 0.5)$ for α_j , $(0.1, 0.3)$ for β_j , $(-5, 5)$ for ν_j , $(0.5, 2)$ for κ_{1j} , $(1.5, 3)$ for κ_{2j} , and $(0.8, 2.5)$ for δ_j , for each $j \in V$. Entries

Algorithm 3.3 Parameter estimation for the MVAGG distribution

- 1: Fix $\Theta_{|i}^d$ at $\hat{\Theta}_{|i}^d$;
 - 2: Initialise $\Theta_{|i}$ and tol ;
 - 3: The current value of $\Theta_{|i}$ is $\Theta_{|i}^*$;
 - 4: Obtain $\hat{\Theta}_{|i}^\Gamma = \underset{\Theta_{|i}^\Gamma}{\operatorname{argmax}} L_{|i} \left(\hat{\Theta}_{|i}^d, \Theta_{|i}^*, \Theta_{|i}^\Gamma \right)$, where $L_{|i}$ is likelihood (3.1);
 - 5: Obtain $\hat{\Theta}_{|i} = \underset{\Theta_{|i}}{\operatorname{argmax}} L_{|i} \left(\hat{\Theta}_{|i}^d, \Theta_{|i}, \hat{\Theta}_{|i}^\Gamma \right)$;
 - 6: **if** $\max(|\hat{\Theta}_{|i} - \Theta_{|i}^*|) > \text{tol}$ **then**
 - 7: set $\Theta_{|i} = \hat{\Theta}_{|i}$;
 - 8: repeat 3. - 5.;
 - 9: **else**
 - 10: **return** $\hat{\Theta}_{|i}$ and $\hat{\Theta}_{|i}^\Gamma$.
 - 11: **end if**
-

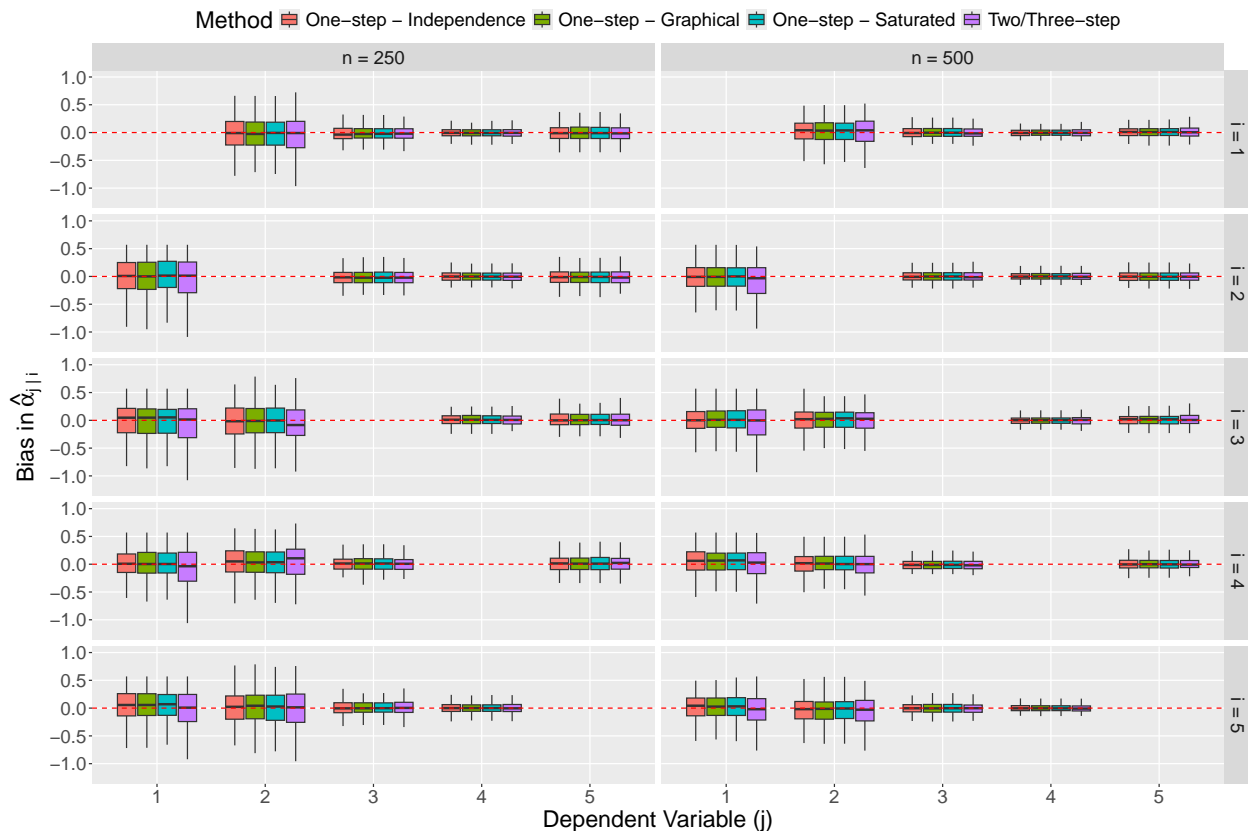


Figure 2: Boxplots detailing the bias of $\hat{\alpha}_{j|i}$ for distinct $i, j \in V$. Each row corresponds to the conditioning variable i , and each column corresponds to the sample size. The fill of the boxplots denotes the different models. The red dashed line indicates the $y = 0$ line.

in $\Sigma_{|i}$ correspond to weak positive associations; see Supplementary Material (Farrell et al., 2024) for examples with weak negative or strong positive associations.

Algorithm 3.4 Graphical selection using the MVAGG SCMEVM

- 1: Initialise ρ ;
 - 2: **for** $i = 1, \dots, d$ **do**
 - 3: Assuming independent Gaussian residuals, obtain $\hat{\Theta}_{|i}^d$ by maximising likelihood (2.2);
 - 4: Using equation (2.3) and $\hat{\Theta}_{|i}^d$, obtain $\hat{z}_{|i}$ and treat them as fixed;
 - 5: Assuming that the components of $\hat{Z}_{|i}$ are independent, obtain $\hat{\Theta}_{|i} = \operatorname{argmax}_{\Theta_{|i}} f_i(\hat{z}_{|i}; \Theta_{|i}, I_{d-1})$ where f_i is given by equation (2.5) and I_{d-1} is a $(d-1)$ -dimensional identity matrix;
 - 6: Set $\Theta_{|i} = \hat{\Theta}_{|i}$ and treating as fixed marginally transform $\hat{z}_{|i}$ onto standard Gaussian margins $\hat{w}_{|i}$;
 - 7: Apply a graphical lasso with penalisation parameter ρ to $\hat{w}_{|i}$ to infer the subgraph $\mathcal{G}_{|i}$;
 - 8: **end for**
 - 9: Obtain a weighted graph \mathcal{G}^* by combining the subgraphs $\mathcal{G}_{|i}$;
 - 10: Create $\hat{\mathcal{G}}$ by pruning the edges of \mathcal{G}^* that do not occur at least 50% of the time;
 - 11: **return** $\hat{\mathcal{G}}$
-

From Algorithm 3.2 the estimates of $\Theta_{|i}^d$ for the SCMEVM are the same across all two- and three-step procedures. Therefore, we restrict our comparison to the one-step (all three structures) and two-step (independence model only) procedures. Figure 2 shows the bias in $\hat{\alpha}_{|i}$ while the Supplementary Material (Farrell et al., 2024) provides comparisons for the remaining parameters, yielding similar findings. Despite using the stepwise procedure, the two-step method converges to the true parameter estimates. When comparing the one- and two-step methods, we find that the former has a slightly narrower range of bias, while the latter has fewer instances of unusually large bias. As expected, the variability in bias decreases as the sample size increases for both procedures.

Table 1 presents the biases of the fitted maximum log-likelihood values. Although the SCMEVMs with graphical or saturated covariance exhibit slightly higher bias than the independent residuals model, the bias is consistent across all three stepwise procedures. Furthermore, we observe that the bias increases with sample size for the independent residual models, while for the graphical and saturated residual models, it remains similar for both $n = 250$ and $n = 500$. This suggests that the structured models are more robust to sample size changes.

Having assessed the accuracy of the stepwise procedures, we now evaluate their computational efficiency. We draw a single realisation from the model for $n \in \{250, 500, 1000, 2000, 4000\}$ excesses above the dependence threshold, and for dimensions $d \in \{5, 10, 15\}$. To enable comparisons across dimensions, the proportion of edges in each graph is set to 60% of its maximum number of edges. Model fitting is performed on a Dell Latitude 7,420 machine

Algorithm 3.5 Simulation of equation (3.2)

- 1: Initialise u ;
 - 2: **for** $l = 1, \dots, N$ such that $N > n$ **do**
 - 3: Draw a conditioning random variable i from $i \in V$ with uniform probability;
 - 4: Simulate $E^l \sim \text{Exp}(1)$ and set $y_i^l = u + E^l$;
 - 5: Simulate $z_{j|i}^l$ from the distribution described in Section 2.2;
 - 6: Calculate $y_{j|i}^l = \hat{\alpha}_{j|i} y_i^l + (y_i^l)^{\hat{\beta}_{j|i}} z_{j|i}^l$ for $j \in V_{|i}$;
 - 7: Calculate an importance weight $w^l = \left(\frac{1}{d} \sum_{m=1}^d \mathbb{1}\{y_m^l > u\} \right)^{-1}$.
 - 8: **end for**
 - 9: Sub-sample n realisations from $\{y^1, \dots, y^N\}$ with probabilities proportional to their importance weights;
 - 10: Transform the sub-sample $\{y^1, \dots, y^n\}$ to $\{x^1, \dots, x^n\}$ via a double application of the PIT;
 - 11: **return** $\{x^1, \dots, x^n\}$
-

Table 1: Median (2.5% and 97.5% quantiles) bias in the fitted maximum log-likelihood values. Bold values denote the least biased stepwise inference procedure for each covariance structure type and conditioning variable.

Covariance Structure		Independent			Graphical			Saturated		
Number of Excesses	Conditioning Variable	One-step	Two-step	Three-step	One-step	Two-step	Three-step	One-step	Two-step	Three-step
250	1	-4.8 (-18.3, 8.7)	-6.2 (-19.3, 8.2)	-6.2 (-19.3, 8.2)	14.0 (7.6, 22.5)	12.8 (6.3, 21.5)	12.7 (6.7 , 21.4)	14.8 (7.6, 25.1)	13.6 (6.4, 24.1)	13.5 (7.0 , 24.0)
	2	-4.2 (-20.6, 11.7)	-4.9 (-18.9, 10.0)	-4.9 (-18.9, 10.0)	14.2 (7.2, 23.6)	11.9 (5.4 , 21.8)	11.9 (5.4 , 21.7)	15.3 (8.0, 25.1)	13.2 (6.4, 23.0)	13.1 (6.2 , 22.9)
	3	0.1 (-11.9, 13.1)	-1.6 (-12.3, 10.7)	-1.6 (-12.3, 10.7)	13.2 (7.1, 22.7)	11.1 (4.7 , 21.3)	11.1 (4.8 , 21.2)	15.1 (7.8, 25.6)	13.2 (5.4 , 24.3)	13.4 (5.6, 24.2)
	4	-3.7 (-18.2, 11.5)	-5.2 (-19.4, 9.9)	-5.2 (-19.4, 9.9)	13.6 (8.2, 21.5)	12.3 (5.9, 20.0)	12.2 (5.9 , 19.9)	14.5 (7.7, 23.1)	13.3 (6.6 , 21.6)	13.3 (6.7 , 21.6)
	5	-13.3 (-34.1, 3.3)	-14.8 (-30.0, 2.3)	-14.8 (-30.0, 2.3)	13.5 (7.6, 22.2)	12.2 (4.7, 21.3)	12.0 (5.3 , 21.0)	14.4 (8.7, 24.1)	12.9 (5.2 , 22.5)	12.9 (6.2 , 22.4)
500	1	-20.9 (-35.9, -4.9)	-22.4 (-39.0, -6.0)	-22.4 (-39.0, -6.0)	14.4 (9.0, 21.3)	12.8 (7.1 , 20.1)	12.8 (7.1 , 20.0)	15.2 (9.1, 22.7)	13.6 (7.6 , 21.0)	13.6 (7.5 , 20.9)
	2	-20.1 (-36.5, -0.3)	-22.0 (-37.0, -2.1)	-22.0 (-37.0, -2.1)	13.8 (7.4, 22.0)	12.0 (4.8, 20.7)	11.9 (5.4 , 20.6)	14.9 (8.4, 23.4)	13.4 (5.9, 22.4)	13.3 (6.0 , 22.3)
	3	-13.4 (-30.9, 2.6)	-16.2 (-31.5, 1.3)	-16.2 (-31.5, 1.3)	13.0 (7.1, 20.9)	10.5 (3.4 , 19.3)	10.6 (3.6, 19.3)	14.9 (8.9, 22.9)	12.9 (5.4, 20.8)	12.8 (5.2 , 20.7)
	4	-17.9 (-33.9, -0.7)	-19.9 (-36.2, -3.8)	-19.9 (-36.2, -3.8)	14.2 (8.2, 24.3)	12.1 (5.0 , 21.3)	12.1 (5.0 , 21.3)	15.1 (8.5, 24.8)	13.2 (5.4 , 22.1)	13.2 (5.4 , 22.0)
	5	-37.0 (-58.1, -18.8)	-39.0 (-60.3, -20.7)	-39.0 (-60.3, -20.7)	13.8 (7.5, 21.9)	12.0 (5.1 , 20.5)	12.0 (5.1 , 20.4)	14.7 (8.6, 24.1)	12.9 (6.3 , 21.7)	13.0 (6.4, 21.6)

with 16GB of RAM, and an 11th generation Intel Core i5 processor with 8 cores. Figure 6 (left panel) shows the time taken in seconds (on the log scale) to fit the one-, two-, and three-step SCMEVMs with graphical and saturated covariance structures. We observe that the one- and two-step methods are considerably slower to fit due to jointly maximising likelihood functions, with at least $6(d-1)$ and $4(d-1)$ parameters per conditioning variable, respectively. Additionally, the high-dimensional parameter space makes it challenging to find starting values for the numerical optimisation. The three-step method is computationally more efficient, showing considerable time savings when n , d , or both, are large.

Table 2: Average time in seconds (2dp) to complete various components of the three-step model fitting procedure for different dimensions.

Inference step	Dimension				
	100	200	300	400	500
Dependence parameters	1.34	2.07	2.84	3.65	4.42
AGG parameters	0.94	1.71	2.65	3.64	4.61
Graphical covariance structure	0.10	0.81	3.61	11.06	30.25
Saturated covariance structure	0.03	0.10	0.22	0.38	0.60

Since Figure 6 (left panel) shows that the three-step procedure with saturated covariance can be quicker to fit than its sparse graphical counterpart, we repeat the study for these two models with $n = 4,000$ and $d \in \{100, 200, 300, 400, 500\}$. We set the proportion of edges in each graph to be 10% of its maximum number of edges. Table 2 shows the average time taken to complete each inference step. As expected, a significant amount of time is spent estimating the graphical structure due to the computational costs of the graphical lasso (Friedman et al., 2007). In contrast, the saturated covariance can be estimated empirically, i.e., no numerical maximisation is required, and the computational cost is primarily from inverting a $(d - 1)$ -dimensional correlation matrix.

4.2 Graphical selection

We now replicate the simulation study of Engelke and Hitz (2020, Section 5.5) to assess how well the SCMEVM identifies the structure \mathcal{G} , shown in Figure 3 (left panel). In this example, $d = 16$ and the data generating mechanism is the Hüsler-Reiss distribution with parameter matrix consistent with \mathcal{G} . The parameters for each of the $p = 18$ edges are sampled independently from a uniform distribution on $(0.5, 1)$, subject to the constraint that the parameter matrix must be conditionally negative definite on cliques with three nodes. We use $n = 100$ replicates of the dataset.

We apply Algorithm 3.4 to infer the optimal graphical structure using the 0.70-quantile of the standard Laplace distribution for the dependence threshold u_{Y_i} . The graphical lasso penalty parameter is set to 0.6. Figure 3 (right panel) shows a weighted graph with line width proportional to the number of times the edge is selected across the 100 datasets. The true graphical structure \mathcal{G} is clearly identified. Moreover, using a majority rule to prune the edges of the weighted graph leaves only one surplus edge compared to the truth. The true graph is recovered by repeating for $\rho \in \{0.60, 0.61, \dots, 0.70\}$ and taking a majority rule over the 11 inferred graphs. Therefore, averaging over multiple penalisation parameters may be beneficial where possible.

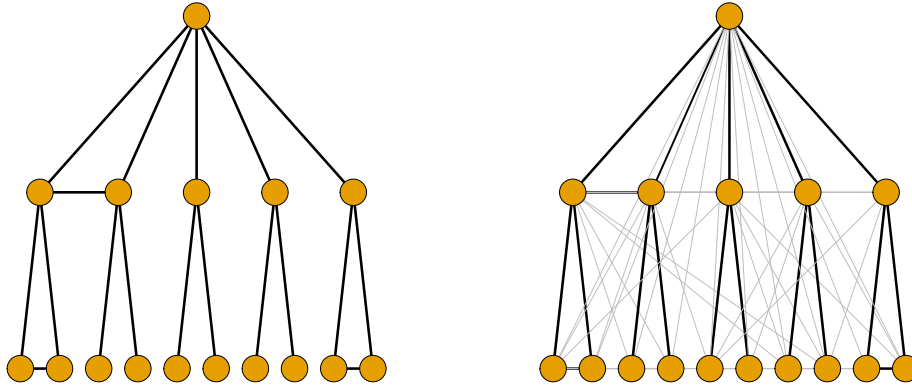


Figure 3: True underlying graphical structure (left) and the inferred graphical structure (right), with line width indicating the number of times each edge was selected across 100 samples. True and misspecified edges are coloured black and grey, respectively.

4.3 Mixture data

To test the general applicability of our model, we use data with a mixture of extremal behaviour. For studies of data with full AI/AD see the Supplementary Material (Farrell et al., 2024). To simulate the mixed data we sample from a 3-dimensional Pareto distribution consistent with a fully connected graph before marginally transforming the data onto standard Gaussian margins, denoted (X_1, X_2, X_3) , using a double application of the PIT. Next, we simulate $(X_4, X_5) \mid X_3 = x_3$ from a conditional Gaussian distribution, such that the precision matrix of (X_3, X_4, X_5) is consistent with a fully connected graph. Then X follows some multivariate distribution with a dependence structure consistent with \mathcal{G} in Section 4.1. A total of $n = 200$ datasets are simulated.

Using Algorithms 3.1 and 3.2, each of the one-, two- and three-step procedures to fit the SCMEVM with graphical covariance. The SCMEVMs with independent and saturated covariances are fitted using the three-step procedure only. For comparison, we also fit the original CMEVM of Heffernan and Tawn (2004) and the graphical extremes model of Engelke and Hitz (2020) (EHM). The dependence threshold u_{Y_i} is the 0.90-quantile of the standard Laplace distribution, with an average of 500 excesses per conditioning variable. We use \mathcal{G} in Section 4.1 for the SCMEVMs with graphical covariance structure and the EHM. Models are compared by their model-based tail probability estimates; true probabilities are obtained from a sample of size 10^6 from the true distribution.

Figure 4 shows empirical and model-based estimates of the conditional precision matrix $\Gamma_{\cdot|i}$.

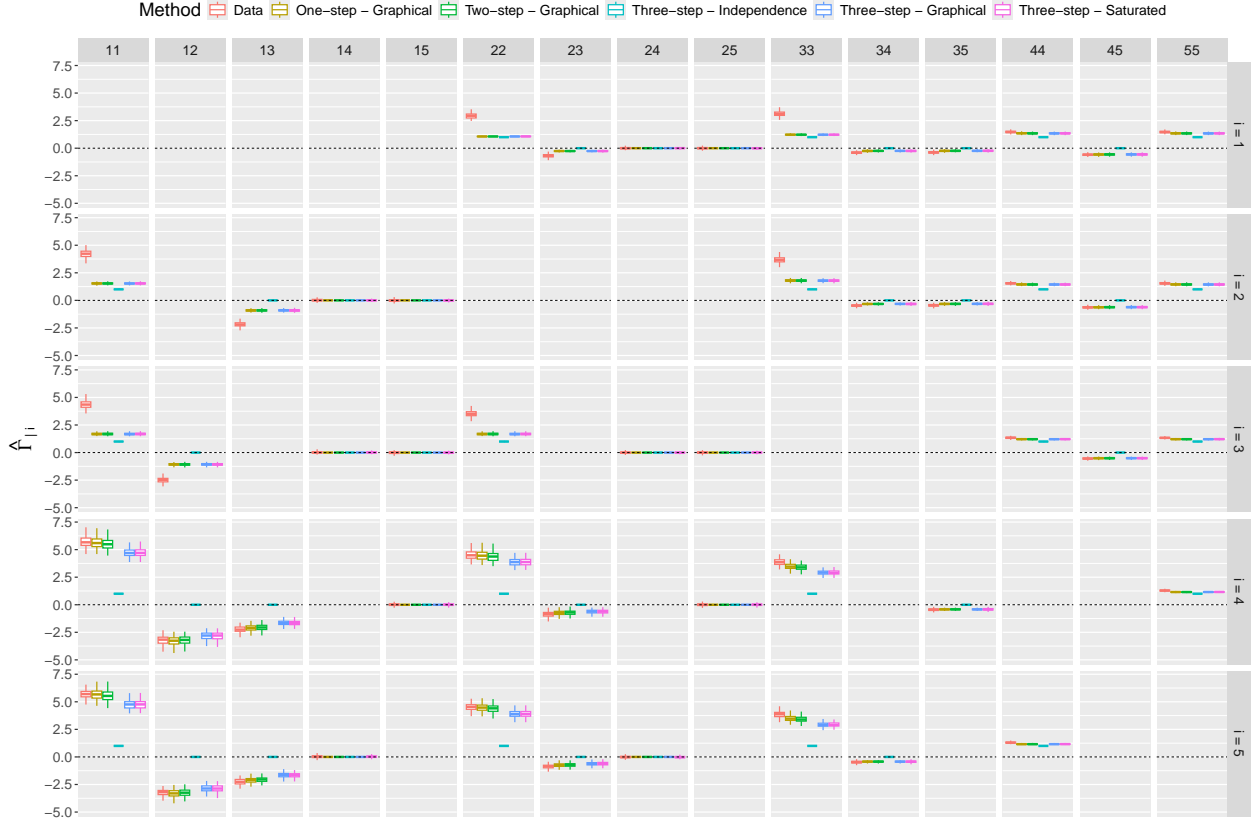


Figure 4: Boxplots of empirical and model-based estimates of $\Gamma_{|i}$, for each $i \in V$, when the data is generated from a mixture distribution. Each row corresponds to the conditioning variable i and each column corresponds to the correlation parameter. The colour of the boxplots distinguishes the different models. The black dashed line indicates the $y = 0$ line.

The empirical estimates are the inverse of the conditional correlation matrix of $Y \mid Y_i = y_i$, where $y_i > u_{Y_i}$ or, equivalently, the inverse correlation matrix of $Y \mid Y_i > u_{Y_i}$ excluding row i and column i . The estimated matrices are almost identical for the graphical and saturated SCMEVMs confirming there is negligible loss in using the former. The estimated structure of the conditional precision matrix from both the graphical and the saturated SCMEVM appears consistent with the empirical version. This suggests that the graphical structure of the residual distribution is inherited from the underlying multivariate distribution, a result that is both consistent with the theoretical findings of Casey and Papastathopoulos (2023) and is also replicated in the cases with full AI/AD (Supplementary Material, Farrell et al. (2024)). Note that the precise values of the non-zero entries in the residual precision matrices cannot be directly compared due to the non-linear transformation (2.1).

Figure 5 shows the bias in the estimates for the tail probabilities $p_1 = \mathbb{P}[X_1 > v, X_2 > v \mid X_3 > v]$ and $p_2 = \mathbb{P}[X_1 > v, X_4 > v \mid X_3 > v]$ where $v = 2.75$. Estimates from the CMEVM are unbiased for both probabilities, while estimates from the SCMEVM with graphical or

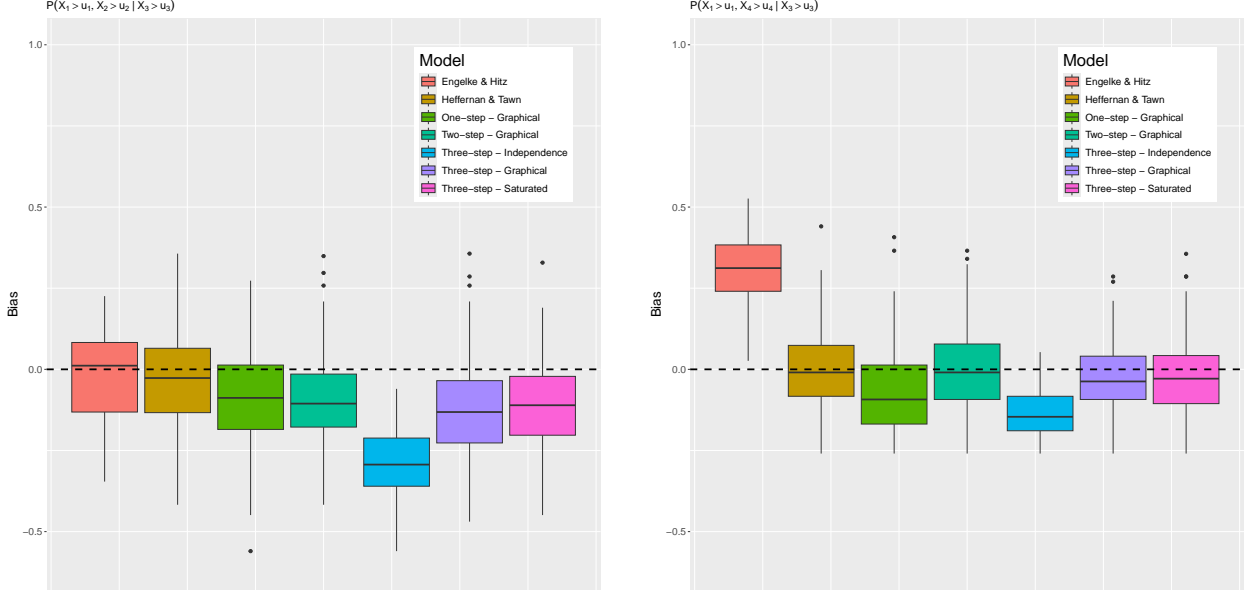


Figure 5: Boxplots of the bias in $p_1 = \mathbb{P}[X_1 > v, X_2 > v \mid X_3 > v]$ (left) and $p_2 = \mathbb{P}[X_1 > v, X_4 > v \mid X_3 > v]$ (right). The fill of the boxplots distinguishes the bias from the different models. The black dashed line indicates the $y = 0$ line.

saturated covariances are unbiased for p_2 , but show slight negative bias for p_1 . Conversely, the EHM estimates of p_1 are unbiased, whereas the estimates of p_2 have considerable positive bias. Similar patterns are seen across the estimates of the remaining 73 conditional probabilities of the form $\mathbb{P}[X_A > v \mid X_i > v]$ for $A \subseteq V_{|i}$ and $i \in V$. Specifically, the SCMEVM is unbiased unless the set $A' = \{A \cup i\}$ has full AD i.e., all $\{\alpha_{j|i} = 1 : j \in A'\}$, while the EHM is unbiased only when A' has full AD. The CMEVM is always unbiased.

Further, if we consider the mean absolute error (MAE) and root mean square error (RMSE) of the estimates for each of the 75 conditional tail probabilities, the SCMEVM vastly outperforms both the EHM and CMEVM, minimising the MAE for 72% of the probabilities and the RMSE for 78% of them. In contrast, the CMEVM (EHM) minimises the MAE 16% (12%) and the RMSE 11% (12%) of the time. This suggests that even for moderate d , the SCMEVM has greater predictive precision and accuracy than the nearest competitor methods.

5 Application

We apply our model to the upper Danube River discharge data described in Section 1. For the margins, we use the empirical-generalised Pareto distribution model from Section 3. The dependence threshold u_{Y_i} used is the 0.80-quantile of the standard Laplace distribution for

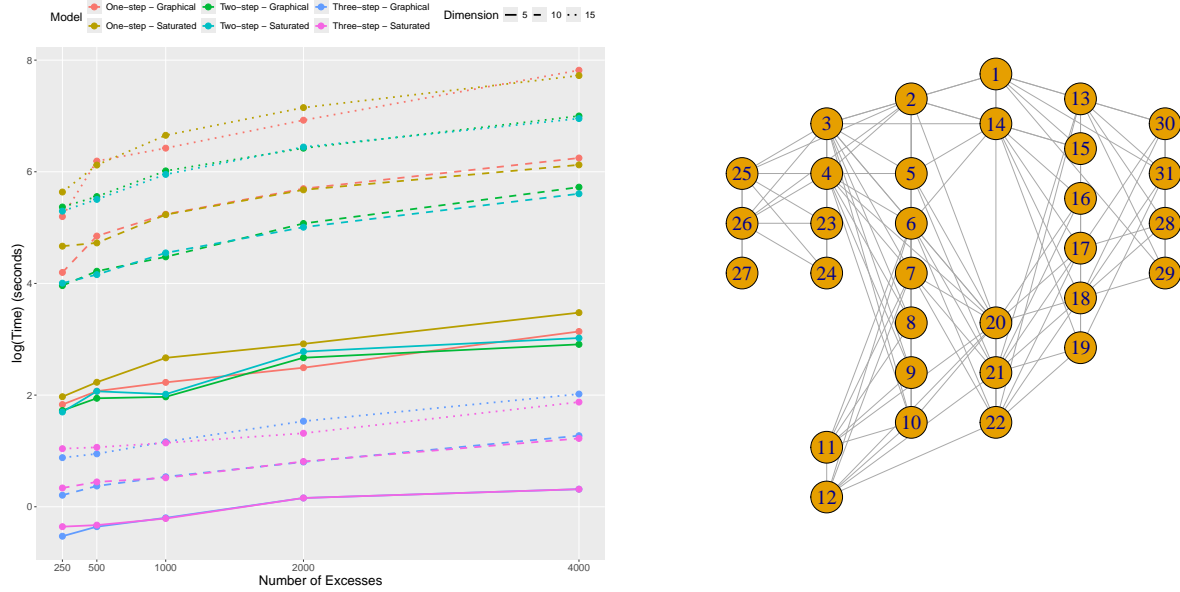


Figure 6: Timing comparison (log scale) of the SCMEVMs (left) for various sample sizes and dimensions, denoted by the line type, and models, denoted by the line colour. Inferred graphical structure of the upper Danube River basin using Algorithm 3.4 (right).

all $i \in V$, resulting in around 85 excesses per station.

We use the three-step procedure to fit the SCMEVM with graphical covariance structure given by the undirected tree induced by the flow connections of the river (Figure 1, left panel); we also fit the EHM with the same structure. Since the flow connection tree may not be the optimal structure for describing the extremes, we also apply the three-step procedure to fit both the SCMEVM with saturated covariance and the SCMEVM with an inferred graphical structure. The inferred graphical structure, obtained from Algorithm 3.4 with $\rho \in \{0.45, \dots, 0.5\}$, is shown in Figure 6 (right panel). This graph has 145 edges compared to the maximum possible 465 edges. Lastly, we simulate datasets from the fitted models using Algorithm 3.5 with $N = 20n$ and $u = u_{Y_i}$.

Bootstrapped estimates of the coefficient of tail dependence $\eta_{i,j}(u)$ for $i, j \in V$, $i > j$ and $u \in \{0.8, 0.85, 0.9\}$ are obtained using 200 bootstrapped samples of the data. For each bootstrapped data set, both empirical and model-based estimates of $\eta_{i,j}(u)$ are obtained. The point estimates in Figure 7 are obtained by taking the medians of the two sets of estimates. The SCMEVMs describe the empirical dependence better than the EHM for both flow-connected (triangles) and flow-unconnected (circles) stations, and across all values of u . This highlights the value of a model that captures a range of extremal dependence classes. Figure 7 shows that all pairs of stations appear to exhibit AI with positive association,

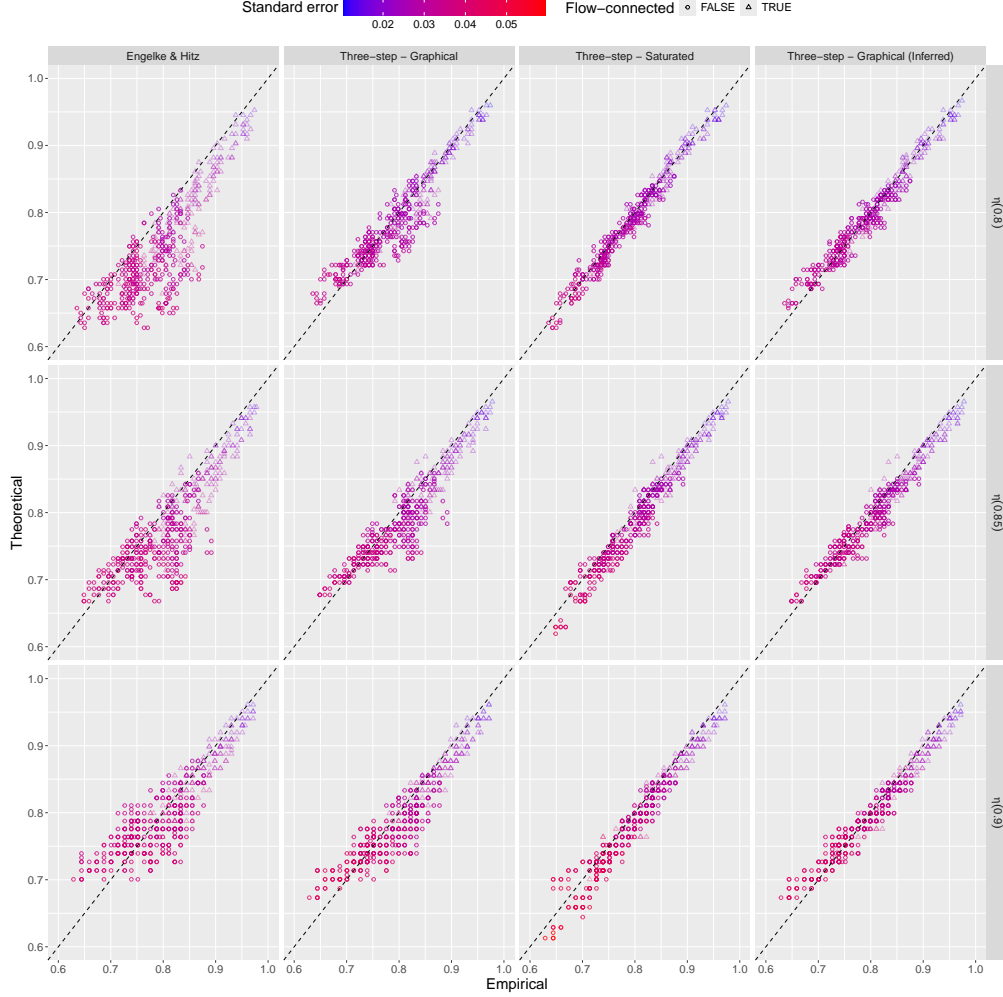


Figure 7: Empirical and model-based estimates of $\eta_{i,j}(u)$ for $u \in \{0.8, 0.85, 0.9\}$ (top to bottom), and $i, j \in V$ but $i > j$. Model-based estimates use the EHM (left) and the three-step SCMEVM with graphical covariance (centre left), with structure given in Figure 1 (left panel), the three-step SCMEVM with saturated covariance (centre right) and graphical covariance (right) with structure given in Figure 6 (right panel). Black dashed lines show $y = x$. Circles (triangles) show flow-connected (flow-unconnected). The colour shows the standard error of the model-based estimates.

$\eta(u) \in (0.5, 1)$, while analogous plots of $\chi(u)$ (Supplementary Material, Farrell et al. (2024)) imply all pairs have AD. However, for stations with weaker (stronger) extremal dependence the two measures decrease (stay close to 1) as u increases. This supports the plausible conclusion that some pairs of stations, particularly those that are flow-unconnected, exhibit AI while others, particularly those that are flow-connected, exhibit AD.

For $u = 0.8$, the SCMEVM with saturated covariance performs noticeably better than the graphical SCMEVM with structure given by the undirected tree induced by the flow connections, suggesting that the extremal dependence is influenced by factors beyond the river

structure (see also Asadi et al. (2015)). To support this hypothesis, Figure 8 shows the bias in the model-based estimates of $\eta_{i,j}(0.8)$ for each pair $i, j \in V$ from the SCMEVM with graphical covariance using the induced undirected tree. From this plot, we see that underestimation predominantly occurs for flow-unconnected stations. For example, the dependence between stations 11-12 and 16-22 is considerably underestimated. While these two sets of stations are flow-unconnected, the sources of their tributaries are geographically close and at similar altitudes, hence stronger dependence than suggested by the lack of flow connection is not unexpected. Similar observations are made when comparing the Isar (stations 14 - 19) and Salzach (stations 28 - 31) tributaries, as well as stations 23 - 24 and 25 - 27. Furthermore, the inferred graphical structure in Figure 6 (right panel) shows many connections between sites on geographically neighbouring tributaries. Indeed, using the inferred graphical structure in the SCMEVM drastically improves the model fit (Figure 7, right panel), and resolves the systematic underestimation caused by using a saturated covariance structure.

Returning to Figure 7, we observe that the SCMEVMs do underestimate dependence at higher thresholds, particularly for flow-unconnected stations with weaker associations. In contrast, the EHM becomes less biased as the threshold increases, although its bias at lower thresholds is greater than the bias in the SCMEVMs at higher thresholds. Moreover, particularly for stations with weaker associations, the cross-site variability in the model-based estimates is much higher for the EHM than the SCMEVMs, regardless of level. In conclusion, the SCMEVMs represent the extremal dependence in the data more accurately and consistently than the EHM.

6 Discussion

In this paper, we have extended the conditional multivariate extreme value model (Heffernan and Tawn, 2004) by replacing the non-parametric residual distribution with a flexible and fully parametric model, overcoming the curse of dimensionality that arises when extrapolating from a non-parametric estimate of a high-dimensional distribution. Our proposed parametric model is the MVAGG distribution. The copula-based construction of the MVAGG, which combines asymmetric generalised Gaussian margins with a multivariate Gaussian dependence structure, facilitates efficient statistical inference, as the margins and dependence structures can be inferred separately in a stepwise manner. Furthermore, graphical structures can be incorporated into the covariance matrix of the multivariate Gaussian distribution in a mathematically tractable way. This provides a simple method to infer the structure if it is not already known, as well as a mechanism to induce sparsity into the dependence structure. Consequently, the model is more general than the spatial model of Richards et al. (2022);

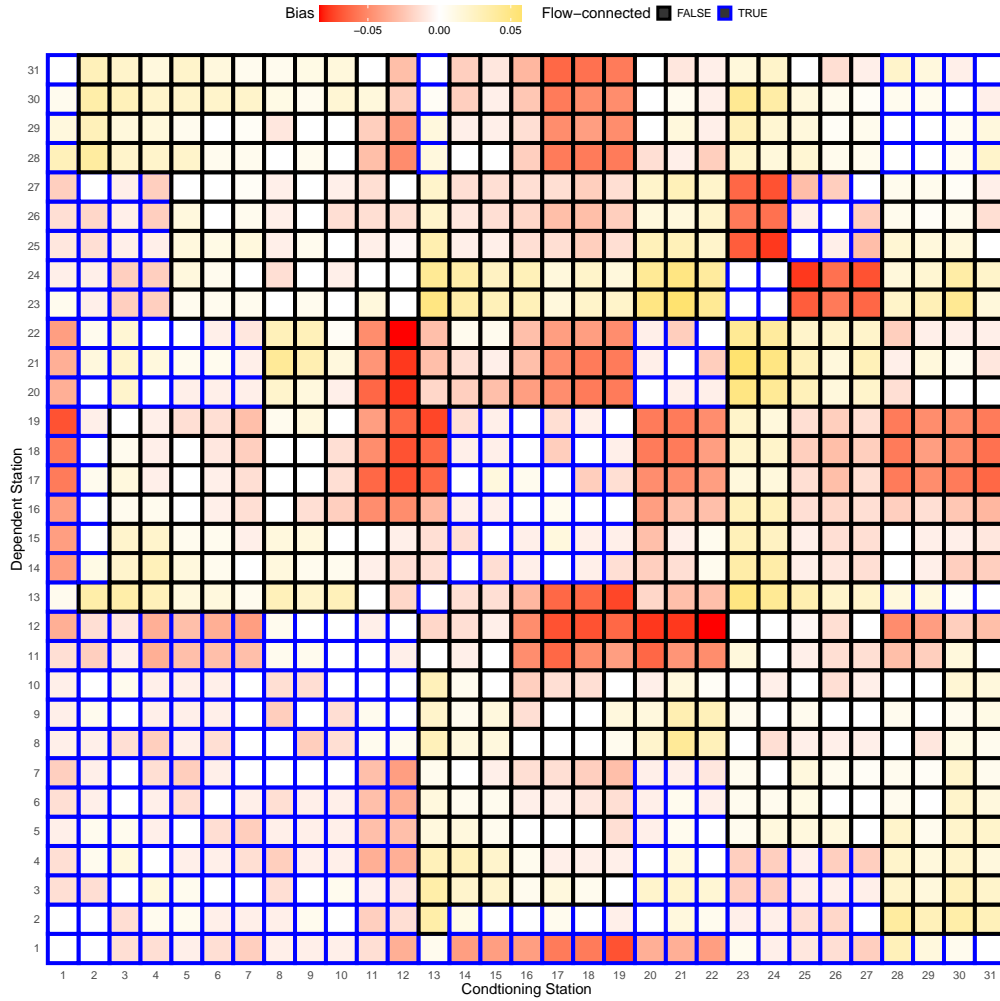


Figure 8: Bias in the median estimates of $\eta_{i,j}(0.8)$ for each $i, j \in V$ for the SCMEVM with a graphical covariance, where the graphical structure is assumed to be the undirected tree induced by the flow connections in Figure 1 (left panel). Under- and over-estimation by the model are represented by red and gold squares, respectively. Flow-connected and flow-unconnected stations are represented by blue and black borders, respectively.

Wadsworth and Tawn (2022), who take a similar copula-based approach but with symmetric generalised Gaussian margins and a less flexible distance-based kernel.

A repercussion of the flexibility of the proposed model is that it has a large parameter space. Separate estimation of the marginal and dependence parameters for the residual distribution is found to be computationally more efficient than joint estimation of all parameters and results in no loss of information.

Nevertheless, despite the sparsity induced by using a graphical structure to model the covariance matrix, fitting this model is more computationally expensive than fitting a model with a saturated covariance structure, since the likelihood for the former must be optimised numerically. Therefore, while graphical structures can be learned and implemented by our model, the model in its current form may not be suitable for very large dimensions. Future work should investigate ways in which the model can be adapted to address this computational hurdle. One approach could be to incorporate factorisation of the residual density using the pairwise Markov structure implied by the graph (Casey and Papastathopoulos, 2023; Engelke and Hitz, 2020). However, this limits the permissible graphical structures to decomposable graphs (Engelke and Hitz, 2020) or chordal graphs where the separator sets are singletons (Casey and Papastathopoulos, 2023).

Our analysis of the upper Danube River basin raises some interesting questions. Firstly, our model captures the dependence between stations more effectively than the multivariate graphical extremes model of Engelke and Hitz (2020), highlighting the need for a flexible model that can capture both AD and AI. However, the implementation of the model using the undirected tree induced by the flow connections of the river network fails to fully capture the extremal dependence in the river discharges. Improved predictions can be obtained either by using the inferred graphical structure or by assuming a saturated covariance matrix. One possible solution to this might be to add a second covariance matrix incorporating geographical spatial structure (Asadi et al., 2015), into the residual distribution of the SCMEVM.

Finally, as with the graphical extremes model of Engelke and Hitz (2020), our model only allows predictions at measured locations. Parameterising the Gaussian copula kernel with a Matérn or Whittle-Matérn correlation function, where distance is defined as the distance along the graph (Bolin et al., 2024), would allow extrapolation to unobserved locations. The generally strong correspondence between the empirical and model-based estimates of η for the flow-connected sites from the SCMEVM gives us confidence that such a model would extrapolate accurately.

Declarations

Funding

Aiden Farrell was supported by the Engineering and Physical Sciences Research Council (EPSRC) grant EP/W523811/1.

Code

Code that supports our findings can be found in the AidenFarrell/Graphical_Conditional_Extremes repository on GitHub.

References

- Asadi, P., Davison, A. C., and Engelke, S. (2015). Extremes on river networks. *The Annals of Applied Statistics*, 9(4):2023 – 2050.
- Blanchet, J. and Davison, A. C. (2011). Spatial modeling of extreme snow depth. *The Annals of Applied Statistics*, 5(3):1699–1725.
- Bolin, D., Simas, A. B., and Wallin, J. (2024). Gaussian Whittle–Matérn fields on metric graphs. *Bernoulli*, 30(2):1611 – 1639.
- Casey, A. and Papastathopoulos, I. (2023). Decomposable Tail Graphical Models. *arXiv preprint arXiv:2302.05182*.
- Coles, S., Heffernan, J., and Tawn, J. (1999). Dependence measures for extreme value analyses. *Extremes*, 2:339–365.
- Davis, R. A., Klüppelberg, C., and Steinkohl, C. (2013). Max-stable processes for modeling extremes observed in space and time. *Journal of the Korean Statistical Society*, 42(3):399–414.
- de Fondeville, R. and Davison, A. C. (2018). High-dimensional peaks-over-threshold inference. *Biometrika*, 105(3):575–592.
- de Haan, L. and Resnick, S. (1987). On regular variation of probability densities. *Stochastic Processes and their Applications*, 25:83–93.
- Debushe, L. K. and Diriba, T. A. (2021). Conditional modelling approach to multivariate extreme value distributions: application to extreme rainfall events in south africa. *Environmental and Ecological Statistics*, 28(3):469–501.

- Engelke, S., Hentschel, M., Lalancette, M., and Röttger, F. (2024a). Graphical models for multivariate extremes. *arXiv preprint arXiv:2402.02187*.
- Engelke, S. and Hitz, A. S. (2020). Graphical models for extremes. *Journal of the Royal Statistical Society: Series B (Statistical Methodology)*, 82(4):871–932.
- Engelke, S., Hitz, A. S., Gnecco, N., and Hentschel, M. (2024b). *graphicalExtremes: Statistical Methodology for Graphical Extreme Value Models*. R package version 0.3.2.
- Engelke, S., Malinowski, A., Kabluchko, Z., and Schlather, M. (2015). Estimation of Hüsler–Reiss distributions and Brown–Resnick processes. *Journal of the Royal Statistical Society Series B: Statistical Methodology*, 77(1):239–265.
- Farrell, A., Eastoe, E. F., and Lee, C. (2024). Supplement to ”Conditional Extremes with Graphical Models”.
- Ferreira, A. and de Haan, L. (2014). The generalized Pareto process; with a view towards application and simulation. *Bernoulli*, 20(4):1717 – 1737.
- Friedman, J., Hastie, T., and Tibshirani, R. (2007). Sparse inverse covariance estimation with the graphical lasso. *Biostatistics*, 9(3):432–441.
- Friedman, J., Hastie, T., and Tibshirani, R. (2019). *glasso: Graphical Lasso: Estimation of Gaussian Graphical Models*. R package version 1.11.
- Gouldby, B., Méndez, F., Guanche, Y., Rueda, A., and Mínguez, R. (2014). A methodology for deriving extreme nearshore sea conditions for structural design and flood risk analysis. *Coastal Engineering*, 88:15–26.
- Gouldby, B., Wyncoll, D., Panzeri, M., Franklin, M., Hunt, T., Hames, D., Tozer, N., Hawkes, P., Dornbusch, U., and Pullen, T. (2017). Multivariate extreme value modelling of sea conditions around the coast of england. *Proceedings of the Institution of Civil Engineers - Maritime Engineering*, 170(1):3–20.
- Heffernan, J. E. and Resnick, S. I. (2007). Limit laws for random vectors with an extreme component. *The Annals of Applied Probability*, 17(2):537 – 571.
- Heffernan, J. E. and Tawn, J. A. (2004). A conditional approach for multivariate extreme values (with discussion). *Journal of the Royal Statistical Society: Series B (Statistical Methodology)*, 66(3):497–546.
- Huser, R. and Davison, A. C. (2014). Space—time modelling of extreme events. *Journal of the Royal Statistical Society. Series B (Statistical Methodology)*, 76(2):439–461.

- Keef, C., Papastathopoulos, I., and Tawn, J. A. (2013). Estimation of the conditional distribution of a multivariate variable given that one of its components is large: Additional constraints for the Heffernan and Tawn model. *Journal of Multivariate Analysis*, 115:396–404.
- Ledford, A. W. and Tawn, J. A. (1996). Statistics for near independence in multivariate extreme values. *Biometrika*, 83(1):169–187.
- Ledford, A. W. and Tawn, J. A. (1997). Modelling dependence within joint tail regions. *Journal of the Royal Statistical Society: Series B (Statistical Methodology)*, 59(2):475–499.
- Murphy, C., Tawn, J. A., and Varty, Z. (2024). Automated threshold selection and associated inference uncertainty for univariate extremes. *Technometrics*, 0(ja):1–17.
- Nacereddine, N. and Goumeidane, A. B. (2019). Asymmetric Generalized Gaussian Distribution Parameters Estimation based on Maximum Likelihood, Moments and Entropy. In *2019 IEEE 15th International Conference on Intelligent Computer Communication and Processing (ICCP)*, pages 343–350.
- Nagler, T. and Czado, C. (2016). Evading the curse of dimensionality in nonparametric density estimation with simplified vine copulas. *Journal of Multivariate Analysis*, 151:69–89.
- Neal, J., Keef, C., Bates, P., Beven, K., and Leedal, D. (2013). Probabilistic flood risk mapping including spatial dependence. *Hydrological Processes*, 27(9):1349–1363.
- Oesting, M. and Stein, A. (2018). Spatial modeling of drought events using max-stable processes. *Stochastic environmental research and risk assessment*, 32:63–81.
- Opitz, T., Huser, R., Bakka, H., and Rue, H. (2018). INLA goes extreme: Bayesian tail regression for the estimation of high spatio-temporal quantiles. *Extremes*, 21(3):441–462.
- R Core Team (2024). *R: A Language and Environment for Statistical Computing*. R Foundation for Statistical Computing, Vienna, Austria.
- Ramos, A. and Ledford, A. (2011). An alternative point process framework for modeling multivariate extreme values. *Communications in Statistics-Theory and Methods*, 40(12):2205–2224.
- Reich, B. J. and Shaby, B. A. (2012). A hierarchical max-stable spatial model for extreme precipitation. *The Annals of Applied Statistics*, 6(4):1430 – 1451.

- Ribatet, M. (2013). Spatial extremes: Max-stable processes at work. *Journal de la Société Française de Statistique*, 154(2):156–177.
- Richards, J., Tawn, J. A., and Brown, S. (2022). Modelling extremes of spatial aggregates of precipitation using conditional methods. *The Annals of Applied Statistics*, 16(4):2693 – 2713.
- Rootzén, H. and Tajvidi, N. (2006). Multivariate generalized Pareto distributions. *Bernoulli*, 12(5):917–930.
- Rootzén, H., Segers, J., and Wadsworth, J. L. (2018). Multivariate generalized Pareto distributions: Parametrizations, representations, and properties. *Journal of Multivariate Analysis*, 165:117–131.
- Ross, E., Astrup, O. C., Bitner-Gregersen, E., Bunn, N., Feld, G., Gouldby, B., Huseby, A., Liu, Y., Randell, D., Vanem, E., and Jonathan, P. (2020). On environmental contours for marine and coastal design. *Ocean Engineering*, 195:106194.
- Schlather, M. (2002). Models for stationary max-stable random fields. *Extremes*, 5:33–44.
- Shooter, R., Ross, E., Ribal, A., Young, I. R., and Jonathan, P. (2021). Spatial dependence of extreme seas in the North East Atlantic from satellite altimeter measurements. *Environmetrics*, 32(4):e2674.
- Shooter, R., Ross, E., Tawn, J., and Jonathan, P. (2019). On spatial conditional extremes for ocean storm severity. *Environmetrics*, 30(6):e2562.
- Simpson, E. S. and Wadsworth, J. L. (2021). Conditional modelling of spatio-temporal extremes for Red Sea surface temperatures. *Spatial Statistics*, 41:100482.
- Simpson, E. S., Wadsworth, J. L., and Tawn, J. A. (2020). Determining the dependence structure of multivariate extremes. *Biometrika*, 107(3):513–532.
- Sklar, M. (1959). Fonctions de répartition à n dimensions et leurs marges. In *Annales de l’ISUP*, volume 8, pages 229–231.
- Smith, R. L. (1990). Max-stable processes and spatial extremes. *Unpublished manuscript*, 205:1–32.
- Smith, R. L., Tawn, J. A., and Coles, S. G. (1997). Markov chain models for threshold exceedances. *Biometrika*, 84(2):249–268.

- Southworth, H., Heffernan, J. E., and Metcalfe, P. D. (2024). *texmex: Statistical modelling of extreme values*. R package version 2.4.9.
- Speed, T. P. and Kiiveri, H. T. (1986). Gaussian Markov Distributions over Finite Graphs. *The Annals of Statistics*, 14(1):138 – 150.
- Stephenson, A. G., Shaby, B. A., Reich, B. J., and Sullivan, A. L. (2015). Estimating spatially varying severity thresholds of a forest fire danger rating system using max-stable extreme-event modeling. *Journal of Applied Meteorology and Climatology*, 54(2):395–407.
- Towe, R., Tawn, J., Lamb, R., and Sherlock, C. (2019). Model-based inference of conditional extreme value distributions with hydrological applications. *Environmetrics*, 30(8):e2575.
- Wadsworth, J. and Tawn, J. (2013). A new representation for multivariate tail probabilities. *Bernoulli*, 19(5B):2689 – 2714.
- Wadsworth, J. and Tawn, J. (2022). Higher-dimensional spatial extremes via single-site conditioning. *Spatial Statistics*, 51:100677.
- Westra, S. and Sisson, S. A. (2011). Detection of non-stationarity in precipitation extremes using a max-stable process model. *Journal of Hydrology*, 406(1-2):119–128.
- Winter, H. C. and Tawn, J. A. (2016). Modelling heatwaves in central france: a case-study in extremal dependence. *Journal of the Royal Statistical Society Series C: Applied Statistics*, 65(3):345–365.
- Winter, H. C. and Tawn, J. A. (2017). k th-order Markov extremal models for assessing heatwave risks. *Extremes*, 20:393–415.

Supplementary Material to “Conditional Extremes with Graphical Models”

S.1 Prediction from the conditional multivariate extreme value model

The original conditional multivariate extreme value model (CMEVM) uses a semi-parametric algorithm for prediction to avoid over-reliance on the working distributional assumptions used for parameter estimation (see Section 2.1 of the main text). Specifically, prediction is performed by non-parametrically sampling with replacement from the empirical distribution of the fitted residuals. Such sampling suffers from the curse of the dimensionality (Nagler and Czado, 2016), meaning the predictive performance of the CMEVM decreases as the dimension increase. To demonstrate this, we perform a simple simulation study and compare the predictive performance of the CMEVM to the structured CMEVM (SCMEVM) proposed in Section 2 of the main text.

Consider a simple undirected graph $\mathcal{G} = (V, E)$ with vertex set $V = \{1, \dots, d\}$ and edge set $E \subseteq \{\{j, k\} \mid j, k \in V, j \neq k\}$ with $\{j, k\} \in E$ if and only if $\{k, j\} \in E$. We set $d = 20$ and randomly select the edges in the graph such that the number of edges is approximately 20% of the number of edges in the full graph. We simulate 200 datasets of size 250 for $Y \mid Y_i > u_{Y_i}$ as per Section 4.1 of the main text i.e., we simulate $Y_i \mid Y_i > u_{Y_i}$ from a standard exponential distribution and obtain $Y_i \mid Y_i > u_{Y_i}$ using equation (2.3) of the main text with Z_i simulated from a multivariate asymmetric generalised Gaussian (MVAGG) distribution (Section 2.2 of the main text). We set the dependence threshold u_{Y_i} to the 0.8-quantile of the standard Laplace distribution. True dependence and asymmetric generalised Gaussian (AGG) parameters are independently sampled from uniform distributions on $(0.1, 0.3)$ for α_j , $(0.1, 0.2)$ for β_j , $(-1, 1)$ for ν_j , $(0.5, 1)$ for κ_{1j} , $(1.5, 2)$ for κ_{2j} , and $(0.8, 2.5)$ for δ_j , for each $j \in V$.

For computational purposes, we consider a single conditioning component i selected at random from V ; similar results can be obtained when conditioning on different components. Predictive performance is assessed on Laplace margins only since the probability integral transform (PIT) used to back-transform to the original margins does not alter the dependence structure. For each data set, we fit the (i) CMEVM, (ii) three-step SCMEVM with graphical covariance structure, and (iii) three-step SCMEVM with saturated covariance. For (ii), the graph is assumed to be known and correctly specified above. For prediction, we used datasets of size 5×10^6 for $Y \mid Y_i > u_{Y_i}$ simulated from the fitted models using the methods

described in Section 4.4 of Heffernan and Tawn (2004) for (i) and Algorithm 1 in Section 5.1 of Wadsworth and Tawn (2022) for (ii) and (iii).

Figure S1 shows $\mathbb{P}[Y_A > v \mid Y_i > v]$, on the exponential scale, for 500 different sets $A \subseteq V_i = V \setminus \{i\}$ such that $|A| = 3$; the sets were chosen at random. We set v to be the 0.999-quantile of the standard Laplace distribution which would approximately correspond to a 1 in 10 year event if we had daily data. The truth is obtained empirically using a single sample of size 10^7 from the true distribution, while the model-based estimates are the median of the model-based point estimates from each of the 200 samples. The CMEVM consistently underestimates the probabilities, whereas the SCMEVMs perform much better, particularly for those probabilities that are very close to 0. The standard error of the model-based estimates (on the original scale), appear to be lower for the SCMEVMs compared to the CMEVM. The SCMEVMs do slightly underestimate the probabilities, however, we anticipate this could be resolved by increasing the size of the prediction datasets.

The CMEVM underestimates the probabilities because it allows neither interpolation nor extrapolation of the fitted residuals, resulting in “rays” in data simulated from the fitted model. This can be seen in Figure S2 which shows 2,000 randomly selected points from data simulated from the fitted models for (i) and (ii). Data used to fit the models is also shown. The CMEVM does not accurately capture dependence between components 2 and 13 but the SCMEVM does much better. This pattern will only be exacerbated as the dimension increases. Therefore the predictive power of the CMEVM will diminish as (1) v approaches the upper end-point of the distribution, (2) the size of set A increases, and (3) the dimension of the problem increases. The SCMEVM overcomes such limitations by using a flexible, fully parametric distribution for the residuals.

S.2 Additional figures and simulation studies for Section 4.1

Section S.2.1 contains additional figures for the simulation study of Section 4.1 in the main text. Also shown are two additional simulation studies to assess the model performance in the presence of either strong positive (Section S.2.2) or weak negative (Section S.2.3) associations. Throughout this section, data are simulated from the SCMEVM with a graphical covariance structure given by $\mathcal{G} = (V, E)$, $V = \{1, \dots, 5\}$, and $E = \{\{1, 2\}, \{1, 3\}, \{2, 3\}, \{3, 4\}, \{3, 5\}, \{4, 5\}\}$.

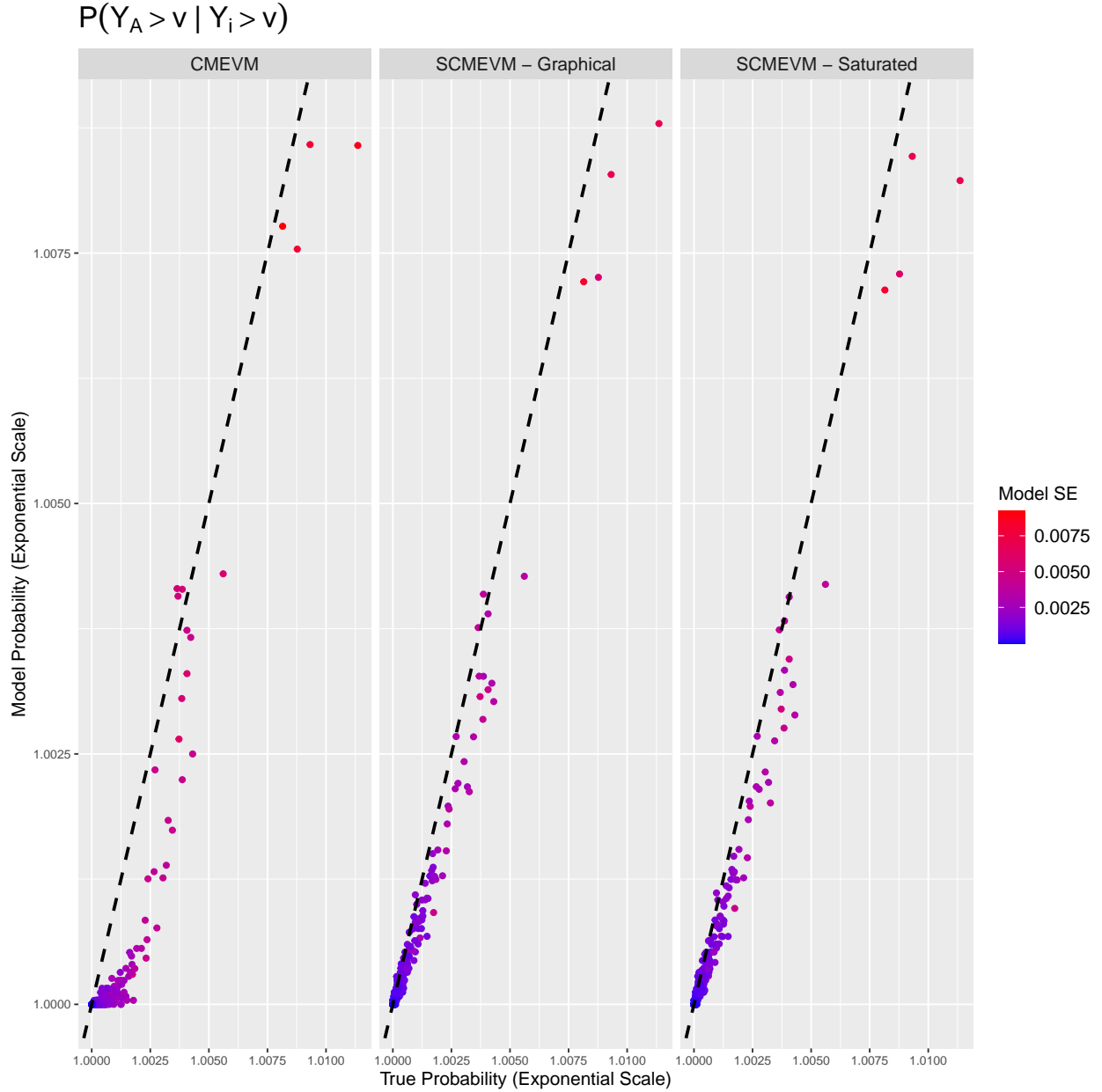


Figure S1: Empirical and model-based estimates of $\mathbb{P}[Y_A > v \mid Y_i > v]$ for a randomly selected component $i \in V$, 500 randomly selected sets $A \subseteq V_i$ such that $|A| = 3$, and v is the 0.999-quantile of the standard Laplace distribution. Model-based estimates use the CMEVM (left), the three-step SCMEVM with graphical covariance (centre) with structure described in Section S.1, and the three-step SCMEVM with saturated covariance (right). The colour shows the standard error of the model-based estimates. Black dashed lines show the $y = x$.

S.2.1 Weak Positive Dependence

For this study, recall that the true dependence and AGG parameters were selected at random by sampling from a uniform distribution on $(0.1, 0.5)$ for α_j , $(0.1, 0.3)$ for β_j , $(-5, 5)$ for ν_j ,

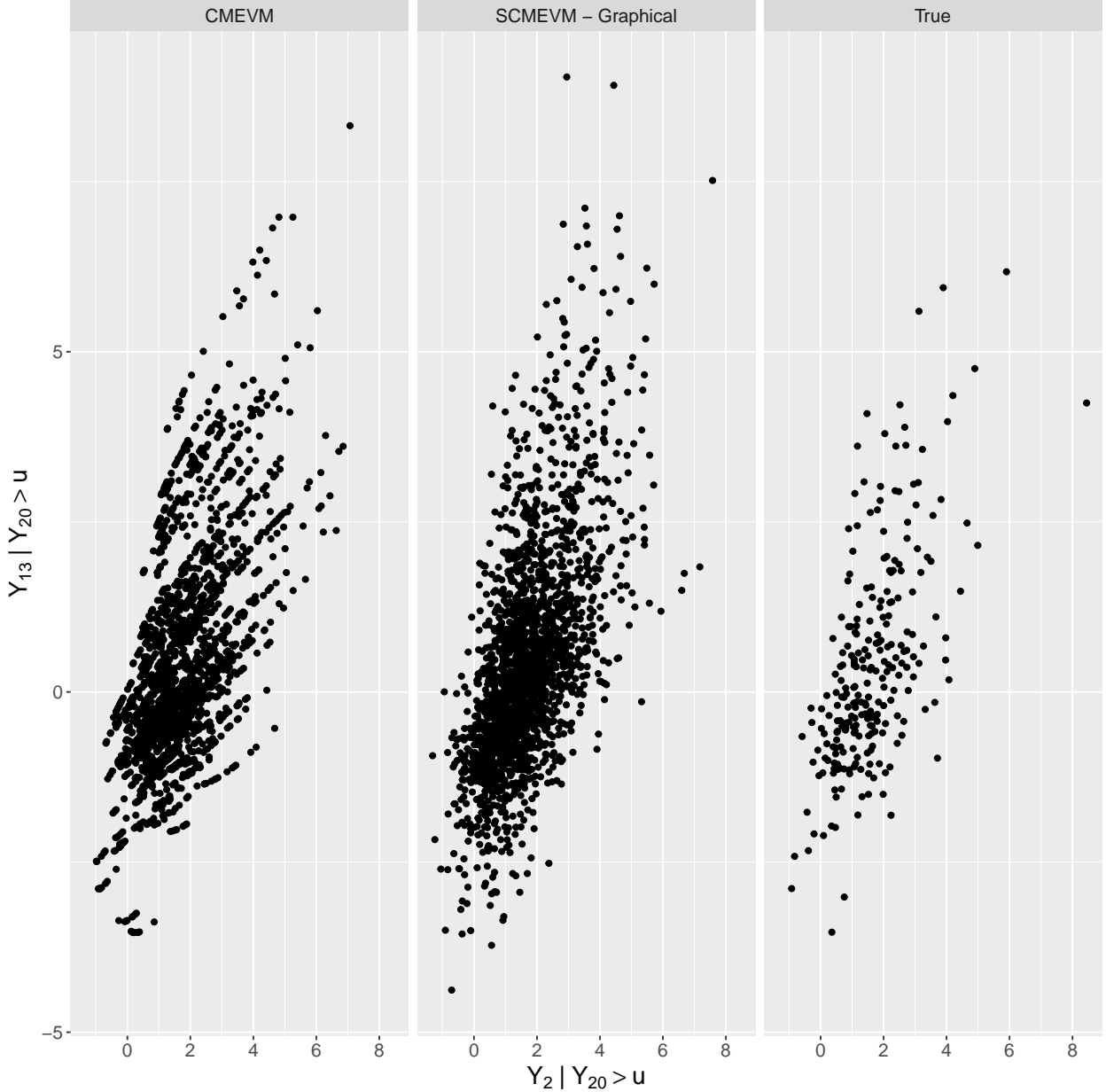


Figure S2: Scatter plots for Y_2 and Y_{13} given $Y_{20} > u_{Y_{20}}$. The points correspond to 2,000 randomly selected data points from a sample of size 5×10^6 simulated from the fitted model for the CMEVM (left), and the three-step SCMEVM with graphical covariance (centre) with structure described in Section S.1. Also shown are the 250 points used to fit the models (right).

$(0.5, 2)$ for κ_{1_j} , $(1.5, 3)$ for κ_{2_j} , and $(0.8, 2.5)$ for δ_j , for each $j \in V$. Figures S3, S4 and S5 show the bias in $\hat{\beta}_{|i}$, the AGG parameters, and $\hat{\Gamma}_{|i}$ respectively. Similar to the plot for $\hat{\alpha}_{|i}$ in the main text, we omit the maximum likelihood estimates (MLEs) from the stepwise methods in cases where they are, by construction, identical to estimates that are already presented. For $\hat{\Gamma}_{|i}$ we exclude those models that assume independent residuals since these are consistently

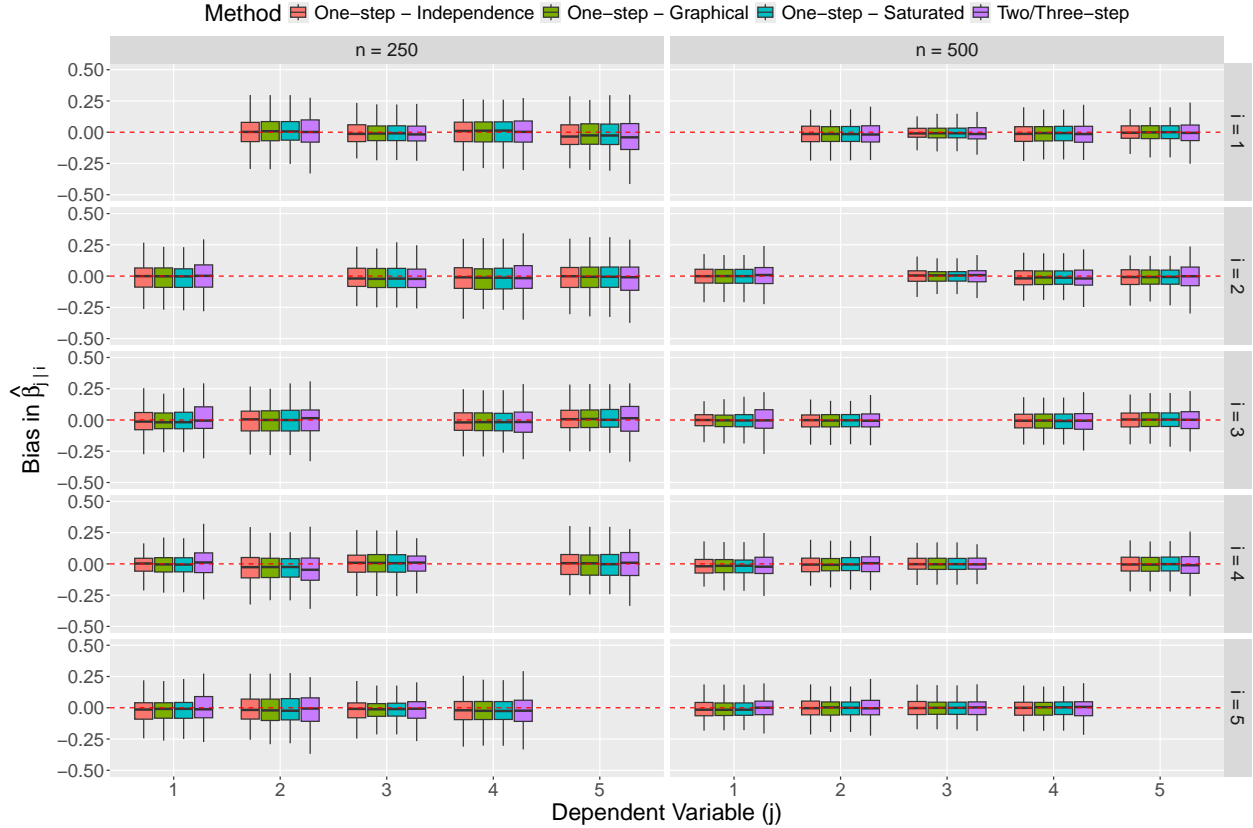


Figure S3: Boxplots detailing the bias of $\hat{\beta}_{j|i}$ for distinct $i, j \in V$. Each row corresponds to the conditioning variable i , and each column corresponds to the sample size. The different models are denoted by the fill of the boxplots. Red dashed lines show $y = 0$.

biased. The findings are very similar to the main text: all models are unbiased across all parameters; the two- and three-step methods show slightly more cross-sample variability in their bias; variability in bias decreases as sample size increases.

S.2.2 Strong Positive Dependence

We repeat the simulation study from Section 4.1 of the main text but with strong, positive correlations (> 0.48). The other parameters remain unchanged from Section S.2.1. Boxplots of the parameter estimates (not included) are almost identical to what was seen with weak positive associations. To compare the three stepwise procedures, we compare the bias in the maximum log-likelihood values, see Table S3. The models with independent residuals are biased; this is expected because the dependence structure is clearly misspecified. The bias is lower in the case when we condition on component 3 because this results in exact independence between (W_1, W_2) and (W_4, W_5) . This result was not seen in the study from the main text due to the lower correlations used there. However, similarly to results shown

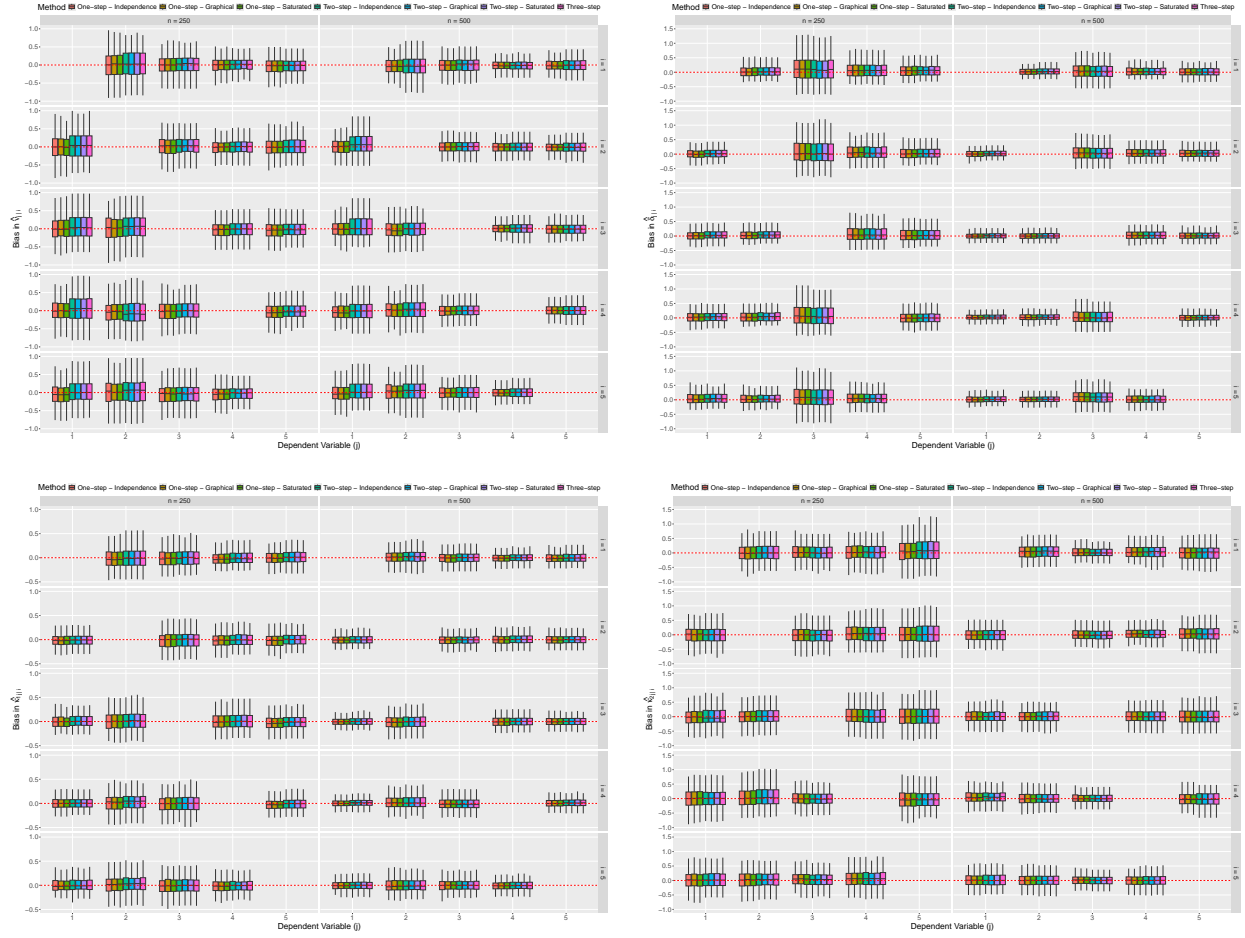


Figure S4: Boxplots detailing the bias of $\hat{\nu}_{j|i}$ (top left), $\hat{\delta}_{j|i}$ (top right), $\hat{\kappa}_{1j|i}$ (bottom left), and $\hat{\kappa}_{2j|i}$ (bottom right) for distinct $i, j \in V$. Each row corresponds to the conditioning variable i , and each column corresponds to the sample size. The different models are denoted by the fill of the boxplots. Red dashed lines show $y = 0$.

in the main text, while models with a graphical or saturated dependence do exhibit a small positive bias, the magnitude of this is similar across all stepwise procedures. This supports our claim that the stepwise inference procedures result in no loss of information. Further, when assuming that the residuals have a graphical or saturated dependence structure, the three-step model is least biased. Finally, the bias for the models with independent residuals increases with the sample size, whereas, the bias from the models with graphical and saturated covariance structures have a similar magnitude of bias for the larger sample size suggesting the latter models are more robust to changes in the sample size.

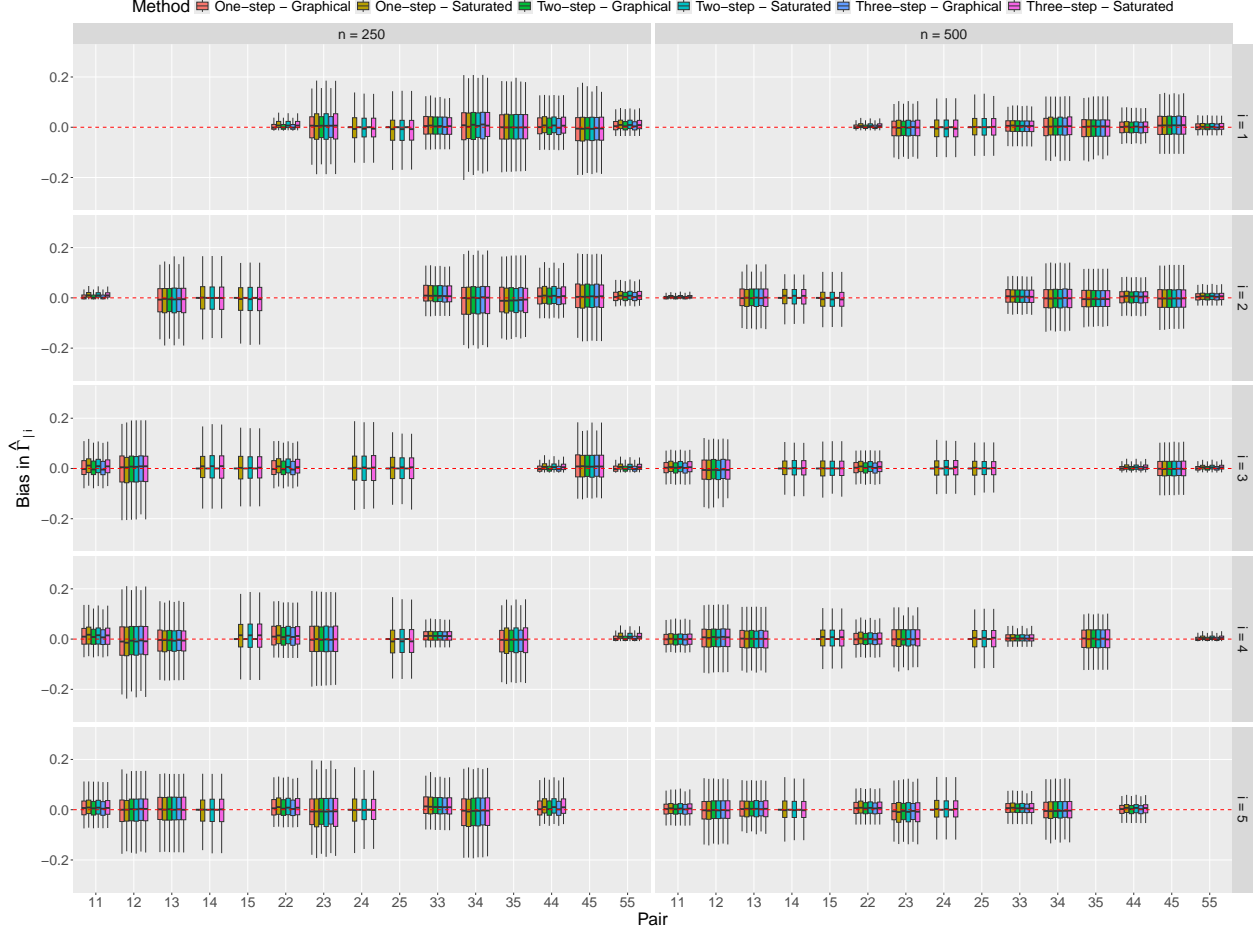


Figure S5: Boxplots for the bias of $\hat{\Gamma}_i$ for each $i \in V$. Each row corresponds to the conditioning variable i , and each column corresponds to the sample size. The various models are denoted by the fill of the boxplots. Red dashed lines show $y = 0$.

Table S3: Median (2.5% and 97.5% quantiles) bias in the fitted maximum log-likelihood values for data from the SCMEVM with strong positive associations. Bold values denote the least biased stepwise inference procedure for each covariance structure type and conditioning variable.

Covariance Structure		Independent			Graphical			Saturated		
Number of Excesses	Conditioning Variable	One-step	Two-step	Three-step	One-step	Two-step	Three-step	One-step	Two-step	Three-step
250	1	-135.7 (-170.2, -98.9)	-137.3 (-171.1, -99.6)	-137.3 (-171.1, -99.6)	14.7 (8.0, 22.5)	12.7 (6.1, 20.8)	11.9 (5.2, 20.6)	15.6 (8.4, 24.0)	13.5 (6.6, 22.1)	12.8 (5.9, 21.4)
	2	-138.5 (-176.4, -100.0)	-139.7 (-172.4, -101.3)	-139.7 (-172.4, -101.3)	14.5 (8.0, 23.0)	11.8 (4.7, 21.6)	11.3 (4.1, 21.0)	15.4 (9.1, 24.8)	12.8 (5.8, 23.2)	12.1 (4.9, 22.3)
	3	-39.8 (-86.1, -18.7)	-41.4 (-59.2, -20.4)	-41.4 (-59.2, -20.4)	13.3 (6.7, 22.8)	11.1 (4.3, 20.6)	11.0 (4.1, 20.3)	15.1 (7.8, 25.7)	13.2 (4.8, 23.6)	13.1 (5.2, 23.2)
	4	-140.0 (-174.1, -94.0)	-140.8 (-175.2, -96.7)	-140.8 (-175.3, -96.7)	14.1 (6.9, 22.9)	11.9 (4.7, 19.3)	11.3 (4.2, 18.7)	15.2 (8.3, 24.1)	12.9 (5.5, 20.6)	12.2 (4.4, 20.2)
	5	-137.5 (-178.1, -105.5)	-137.8 (-174.8, -106.5)	-137.8 (-174.8, -106.5)	14.0 (8.0, 22.6)	11.5 (3.2, 20.8)	10.7 (2.8, 20.5)	15.1 (8.9, 24.3)	12.5 (4.8, 22.1)	11.8 (4.4, 21.7)
500	1	-280.2 (-326.7, -226.3)	-281.9 (-327.7, -228.3)	-281.9 (-327.7, -228.3)	13.7 (7.6, 21.1)	11.9 (5.3, 19.2)	11.2 (4.7, 18.3)	14.7 (8.7, 22.2)	13.0 (6.2, 20.7)	12.1 (5.6, 19.9)
	2	-286.9 (-332.7, -240.5)	-289.0 (-333.7, -242.0)	-289.0 (-333.7, -242.0)	13.7 (7.7, 22.8)	11.0 (3.3, 19.5)	10.5 (2.6, 18.7)	14.7 (7.6, 24.1)	11.7 (3.8, 21.3)	11.3 (3.1, 20.3)
	3	-95.3 (-126.8, -67.7)	-97.1 (-123.7, -71.9)	-97.1 (-123.7, -71.9)	12.9 (7.1, 21.3)	10.3 (3.7, 18.7)	10.1 (3.5, 18.3)	14.8 (8.0, 23.4)	12.3 (4.5, 20.6)	12.1 (4.9, 20.1)
	4	-282.0 (-332.8, -229.4)	-283.7 (-333.4, -231.2)	-283.7 (-333.4, -231.2)	14.0 (8.5, 21.1)	11.4 (1.9, 19.2)	10.9 (1.0, 18.7)	14.9 (9.3, 23.6)	12.5 (2.0, 20.6)	11.8 (1.2, 19.8)
	5	-286.3 (-342.2, -234.9)	-286.9 (-338.3, -236.3)	-286.9 (-338.3, -236.3)	14.1 (7.4, 20.7)	11.3 (2.1, 18.4)	10.7 (1.4, 17.6)	14.9 (8.1, 22.3)	12.4 (4.2, 20.4)	11.7 (2.8, 19.2)

S.2.3 Negative Dependence

Similar to Section S.2.2, we repeat the simulation from Section 4.1 of the main text but with negative associations between some components. Equation (S.1) shows the true correlation

Table S4: Median (2.5% and 97.5% quantiles) bias in the fitted maximum log-likelihood values for data from the SCMEVM with weak negative associations. Bold values denote the least biased stepwise inference procedure for each covariance structure type and conditioning variable.

Covariance Structure		Independent			Graphical			Saturated		
Number of Excesses	Conditioning Variable	One-step	Two-step	Three-step	One-step	Two-step	Three-step	One-step	Two-step	Three-step
250	1	-13.3 (-26.7, 1.0)	-14.2 (-27.6, -0.4)	-14.2 (-27.6, -0.4)	13.9 (8.0, 22.7)	12.5 (6.1, 21.7)	12.4 (6.0, 21.6)	14.9 (8.1, 27.0)	13.2 (6.8, 24.8)	13.1 (7.0, 24.8)
	2	-11.6 (-28.4, 3.8)	-13.3 (-27.6, 1.3)	-13.3 (-27.6, 1.3)	14.6 (7.5, 23.4)	12.6 (3.3, 20.6)	12.7 (4.8, 21.4)	15.9 (7.6, 25.1)	13.6 (4.6, 23.5)	13.6 (5.5, 23.1)
	3	-13.3 (-46.8, 2.3)	-14.6 (-28.7, 2.5)	-14.6 (-28.7, 2.5)	13.6 (6.9, 23.4)	11.3 (4.6, 21.0)	11.2 (4.6, 20.8)	15.6 (8.1, 26.3)	13.1 (5.2, 23.9)	13.0 (5.7, 23.7)
	4	-12.9 (-48.7, 1.6)	-14.3 (-26.4, -0.2)	-14.3 (-26.4, -0.2)	13.8 (7.3, 21.9)	12.3 (5.4, 20.5)	12.2 (5.9, 20.3)	14.6 (5.1, 23.2)	13.0 (6.7, 21.6)	12.9 (6.8, 21.6)
	5	-19.7 (-35.6, -4.7)	-21.0 (-35.7, -5.7)	-21.0 (-35.7, -5.7)	13.6 (7.3, 21.9)	12.0 (4.7, 20.2)	12.0 (4.9, 20.0)	14.7 (8.1, 23.6)	13.1 (5.7, 22.3)	13.0 (5.6, 22.1)
500	1	-37.6 (-59.8, -20.8)	-38.8 (-61.0, -22.2)	-38.8 (-61.0, -22.2)	14.4 (8.9, 22.7)	12.9 (6.1, 20.8)	12.8 (6.0, 20.7)	15.1 (9.4, 23.2)	13.8 (6.9, 21.5)	13.7 (6.8, 21.4)
	2	-34.9 (-57.8, -12.8)	-36.9 (-59.3, -13.1)	-36.9 (-59.3, -13.1)	14.3 (7.7, 23.1)	12.3 (4.4, 21.7)	12.2 (4.3, 21.5)	15.1 (8.5, 24.0)	13.2 (5.4, 22.8)	13.1 (5.3, 22.5)
	3	-33.8 (-51.9, -15.4)	-35.4 (-54.2, -17.1)	-35.4 (-54.2, -17.1)	13.1 (6.9, 20.3)	10.7 (2.1, 18.6)	10.6 (2.5, 18.5)	14.8 (8.2, 23.0)	12.3 (3.1, 20.3)	12.3 (3.0, 20.2)
	4	-40.5 (-57.8, -19.5)	-41.7 (-59.7, -20.9)	-41.7 (-59.7, -20.9)	13.9 (8.2, 22.9)	11.9 (5.1, 20.6)	11.7 (5.0, 20.5)	14.7 (9.1, 24.1)	12.8 (5.4, 21.9)	12.7 (5.4, 21.7)
	5	-51.2 (-70.9, -31.4)	-52.8 (-70.6, -33.2)	-52.8 (-70.6, -33.2)	13.8 (8.5, 22.6)	12.0 (5.3, 21.3)	11.9 (5.1, 20.9)	14.5 (9.3, 23.9)	12.9 (6.4, 22.3)	12.7 (6.2, 22.0)

matrix. All other parameters remain unchanged from Section S.2.1.

$$\Sigma = \begin{bmatrix} 1.000 & -0.308 & -0.134 & 0.034 & 0.019 \\ -0.308 & 1.000 & -0.160 & 0.041 & 0.023 \\ -0.134 & -0.160 & 1.000 & -0.254 & -0.141 \\ 0.034 & 0.041 & -0.254 & 1.000 & -0.209 \\ 0.019 & 0.023 & -0.141 & -0.209 & 1.000 \end{bmatrix} \quad (\text{S.1})$$

Parameter estimates have been omitted as they were similar to those presented for the weak positive association example in the main text. To compare the stepwise inference procedures, Table S4 gives the biases of the fitted maximum log-likelihood values. As in the strong positive association study (Section S.2.2), models with independent residuals have negative bias that increase with the sample size, while those with graphical or saturated dependence have small positive bias that is impervious to the sample size. Again, the magnitude of the bias is similar across all stepwise procedures, confirming no loss of information in using these.

S.3 Additional figures and simulation studies for Section 4.3

In the main text, we considered data with a mixture of extremal dependence structures. We now repeat the simulation study in Section 4.3 of the main text for data that exhibits either full asymptotic independence (AI) or full asymptotic dependence (AD). For AI, we simulate from each of the (a) multivariate Gaussian (MVG), (b) symmetric multivariate Laplace (MVL), and (c) multivariate t - (MVT) distributions. In all cases, both positive and negative associations are investigated. For AD, we simulate from a multivariate Pareto (MVP) distribution. All simulation studies follow a similar pattern. For each true distribution, 200 datasets are sampled using a dependence structure consistent with \mathcal{G} in Section S.2. Data are

transformed from their canonical margins (e.g., Gaussian for the MVG distribution) to standard Laplace margins as per Section 3.1 of the main text. For all data sets, each of the one-, two- and three-step procedures is used to fit the SCMEVM with graphical covariance, where the graph is assumed to be known and correctly specified. The three-step procedure is also used to fit the SCMEVM with independent and saturated covariances. For comparison, we also fit the original CMEVM (Heffernan and Tawn, 2004) and the graphical extremes model (Engelke and Hitz, 2020) (EHM). The mean absolute error (MAE) and root mean squared error (RMSE) of the model-based estimates form the basis of model comparison. For simulations that have positive associations, we use tail probabilities $\mathbb{P}[X_A > u_{X_A} \mid X_i > u_{X_i}]$ (for all sets $A \subseteq V_i$ and $i \in V$) for model comparison, while for those that have negative associations we use probabilities of the form $\mathbb{P}[X_A < u_{X_A} \mid X_i > u_{X_i}]$ for model comparison.

S.3.1 Multivariate Gaussian Distribution

In this section, we assume X follows a MVG distribution with mean vector $\boldsymbol{\mu}$, where each μ_j is independently sampled from a uniform distribution on $(-5, 5)$, and correlation matrix Σ . Various strengths of correlation are considered however $\Gamma = \Sigma^{-1}$ is always consistent with \mathcal{G} in Section S.2. We set dependence thresholds u_{Y_i} to the 0.90-quantile of the standard Laplace distribution. For prediction, we set u_{X_i} to the 0.95-quantile for the true distribution of X_i for each $i \in V$.

S.3.1.1 Weak Positive Dependence

In the first study, correlations between all components lie in $(0, 0.47)$. Figure S6 shows MLEs of the dependence and AGG parameters. Here, and in the other studies in this section, estimates from the three-step SCMEVM with graphical and saturated covariance structures are omitted as they are identical to results for the three-step SCMEVM with independent residuals. Also note that the MLEs for CMEVM dependence parameters are the same for the two- and three-step methods. The MLEs of $\boldsymbol{\alpha}_{|i}$ ($\boldsymbol{\nu}_{|i}$) from the one-step procedure are consistently lower (higher) than the MLEs from the stepwise approaches, confirming that the one-step method does not guarantee that the first-order extremal dependence structure will be captured by the dependence parameters. At best, by attributing some extremal dependence structure to the residual distribution, the interpretability of the SCMEVMs fitted with the one-step procedure is reduced. Potentially, it also makes the models less reliable. In contrast, the MLEs of $\boldsymbol{\beta}_{|i}$, $\boldsymbol{\kappa}_{1|i}$, $\boldsymbol{\kappa}_{2|i}$, and $\boldsymbol{\delta}_{|i}$ are similar across all the models and fitting procedures. Finally, the right-scale parameter $\kappa_{2|j|i}$ is almost always estimated to be larger than the left-scale parameter $\kappa_{1|j|i}$, supporting the choice of an asymmetric marginal distribution for $Z_{|i}$.

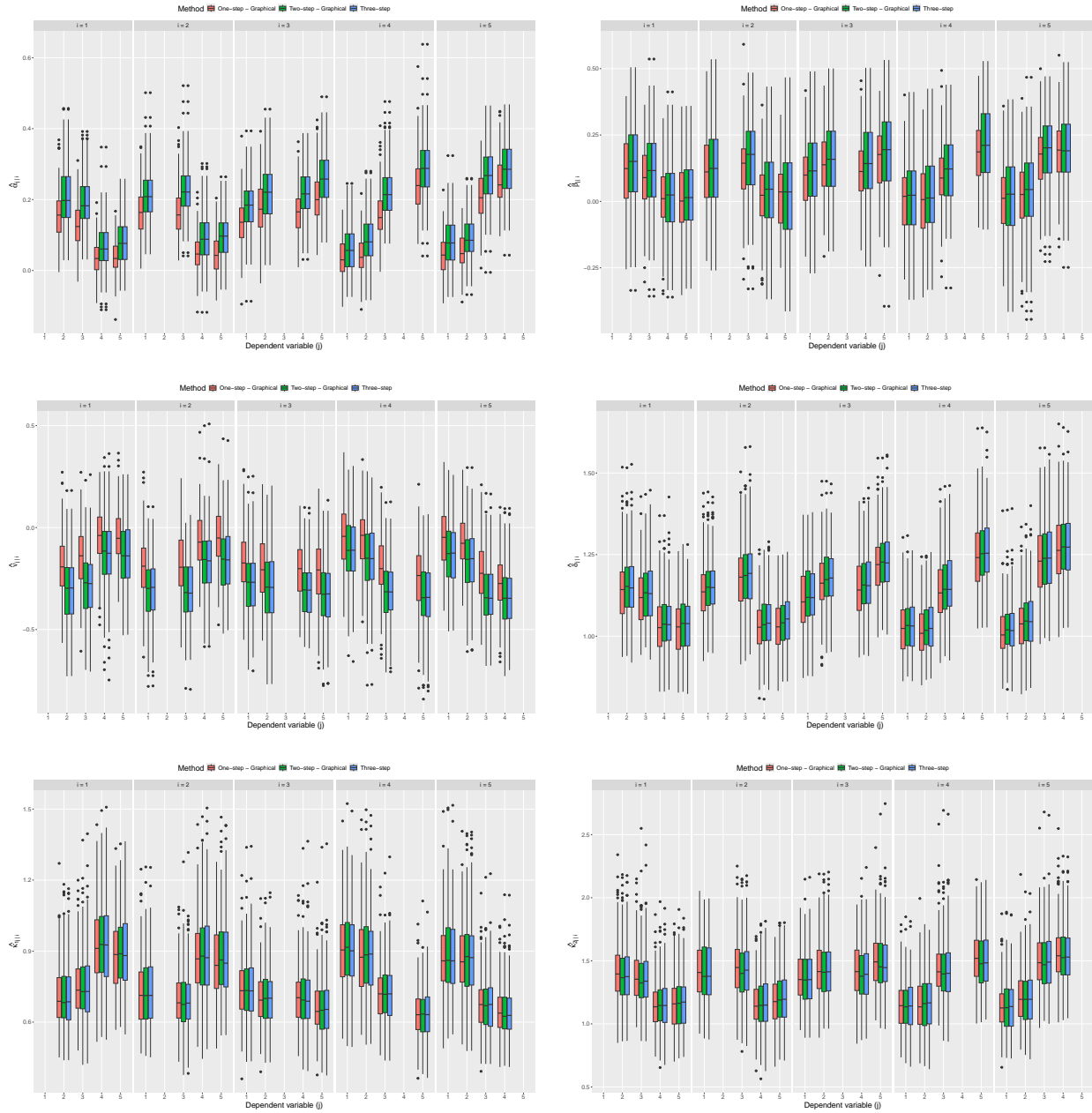


Figure S6: Boxplots of MLEs for $\alpha_{j|i}$ (top left), $\beta_{j|i}$ (top right), $\nu_{j|i}$ (centre left), $\delta_{j|i}$ (centre right), $\kappa_{1j|i}$ (bottom left), and $\kappa_{2j|i}$ (bottom right) for distinct $i, j \in V$. Each row corresponds to the conditioning variable i . The different models are denoted by the fill of the boxplots.

Figure S7 shows empirical and model-based estimates of the conditional precision matrix $\Gamma_{|i}$. Empirical estimates are the inverse of the conditional correlation matrix for $Y \mid Y_i = y_i$, such that $y_i > u_{Y_i}$, equivalently the inverse correlation matrix of $Y \mid Y_i > u_{Y_i}$ excluding the i th row and column. Similar to the study in the main text, the estimated matrices are the same for the graphical and saturated SCMEVMs confirming there is negligible loss in using the former.



Figure S7: Boxplots of empirical and model-based estimates of $\Gamma_{i|}$, for each $i \in V$, when the data is generated from a MVG distribution with weak positive associations. Each row corresponds to the conditioning variable i and each column corresponds to the correlation parameter. The different models are denoted by the colour of the boxplots. Black dashed lines show $y = 0$.

Further the estimated structure of the conditional precision matrices for the graphical and saturated SCMEVMs is consistent with the empirical version. While it is plausible that the results here are specific to the MVG generating mechanism, similar patterns are observed for the other multivariate distributions.

We now compare predictions from the EHM and three-step SCMEVM with graphical covariance. Figure S8 (left panel) shows the bias in the conditional survival curves of $X_j | X_1 > u_{X_1}$ for each $j \in V_{|1}$. The SCMEVM is unbiased for all curves whereas the EHM has positive bias for lower values of u_{X_j} ; this decreases as u_{X_j} increases. The positive bias of the EHM persists in bivariate conditional survival probabilities. Figure S8 (right panel) shows the bias in $\mathbb{P}[X_2 > u_{X_2}, X_3 > u_{X_3} | X_1 > u_{X_1}]$. The three-step SCMEVM with independent residuals exhibits negative bias because X_2 is not conditionally independent of X_3 given X_1 . In contrast, the SCMEVMs with graphical and saturated covariances are unbiased. The CMEVM predictions are also unbiased, probably due to the low dimension d . Lastly, the SCMEVMs with

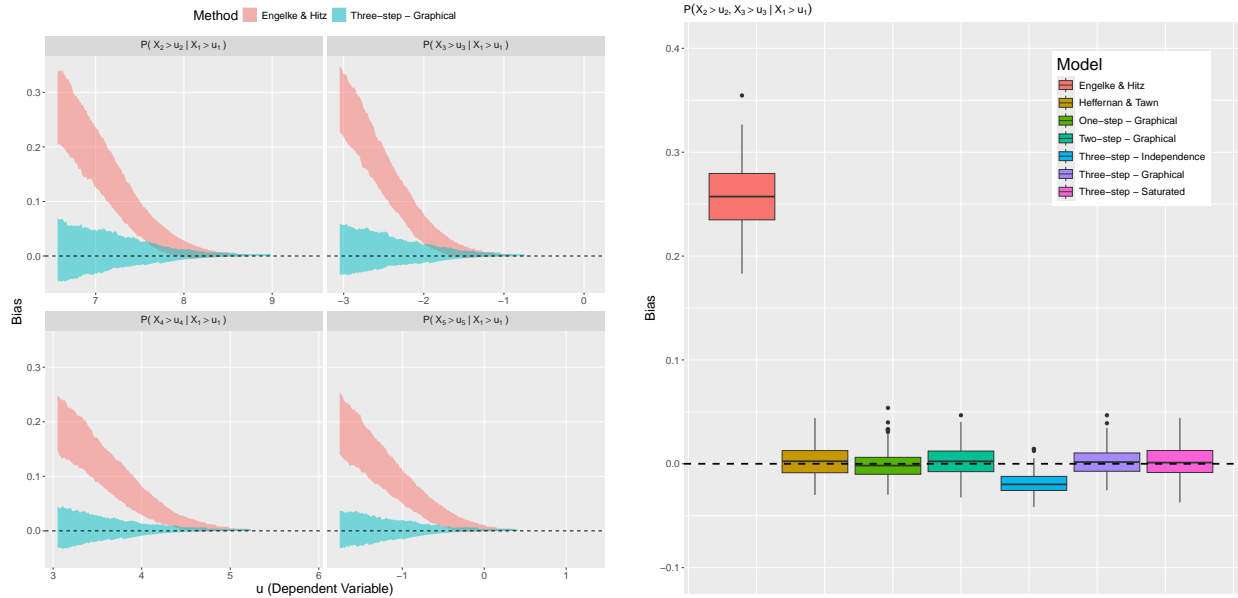


Figure S8: Polygon plots detailing 95% confidence intervals, over 200 samples, of the bias in $\mathbb{P}[X_j > u_{X_j} \mid X_1 > u_{X_1}]$, for each $j \in V_{|1}$, where X follows a MVG distribution with weak positive associations (left). The bias from the EHM and the three-step SCMEVM assuming a graphical covariance structure for the residuals are in pink and blue, respectively. Boxplots of the bias in $\mathbb{P}[X_2 > u_{X_2}, X_3 > u_{X_3} \mid X_1 > u_{X_1}]$ (right). The bias from the various models is denoted by the fill of the boxplots. Black dashed lines show $y = 0$.

graphical covariance exhibit the least amount of bias and variability, minimising the MAE and RMSE for 87% and 77% of the 75 conditional probabilities, respectively. This confirms that there is no loss in performance when using a graphical structure over the more flexible saturated one and that the fully parametric SCMEVM outperforms the semi-parametric CMEVM. The EHM performs badly in this case because the true data have AI.

S.3.1.2 Strong Positive Dependence

We repeat the simulation study in Section S.3.1.1 but the associations between the components of X are strong and positive (> 0.52). We present only the predictive performances, as the parameter estimates show similar patterns to those seen in Section S.3.1.1. Figure S9 (left panel) shows bias in the conditional survivor curves for $X_j \mid X_5 > u_{X_5}$ for both the EHM and the three-step SCMEVM with a graphical covariance structure, for $j \in V_{|5}$. Again, the EHM is biased for low values of u_{X_j} but this diminishes as u_{X_j} increases; the three-step SCMEVM with graphical structure is unbiased for all u_{X_j} . Figure S9 (right panel) shows the bias in $\mathbb{P}[X_{|5} > u_{X_{|5}} \mid X_5 > u_{X_5}]$. The EHM has positive bias whereas both the CMEVM and the SCMEVMs with graphical or saturated covariance structures are unbiased. The three-step SCMEVM with independent residuals has negative bias; this is expected since the compo-

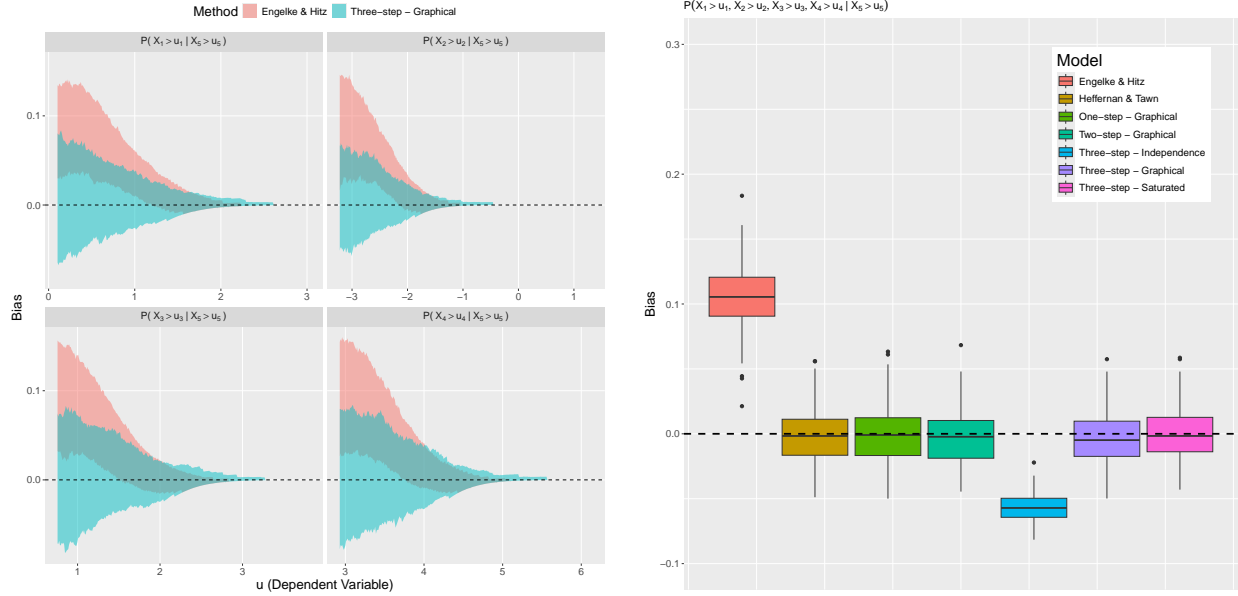


Figure S9: Polygon plots detailing 95% confidence intervals, over 200 samples, of the bias in $\mathbb{P}[X_j > u_{X_j} \mid X_5 > u_{X_5}]$, for $j \in V_{|5}$ where X follows a MVG distribution with strong positive associations (left). The bias from the EHM and the three-step SCMEVM with a graphical covariance structure are in pink and blue, respectively. Boxplots of the bias in $\mathbb{P}[X_{|5} > u_{X_{|5}} \mid X_5 > u_{X_5}]$ (right). The bias from the various models is denoted by the fill of the boxplots. Black dashed lines show $y = 0$.

nents of $X_{|5}$ are not independent given X_5 is large. Assessing overall predictive performance, the SCMEVMs with graphical covariance structure are again the least biased and variable, minimising the MAE and RMSE metrics 81% and 84% of the time, respectively.

S.3.1.3 Negative Dependence

We repeat the simulation study in Section S.3.1.1 but the association between the components of X are now allowed to be negative. The correlation matrix Σ is given in equation (S.1).

$$\Sigma = \begin{bmatrix} 1.000 & -0.468 & -0.370 & -0.136 & 0.134 \\ -0.468 & 1.000 & 0.390 & 0.144 & -0.141 \\ -0.370 & 0.390 & 1.000 & 0.369 & -0.362 \\ -0.136 & 0.144 & 0.369 & 1.000 & -0.346 \\ 0.134 & -0.141 & -0.362 & -0.346 & 1.000 \end{bmatrix} \quad (\text{S.1})$$

Figure S10 compares the MLEs of $\kappa_{1|j|i}$ and $\kappa_{2|j|i}$ from the three-step SCMEVM with a graphical covariance structure, for distinct $i, j \in V$. In the other MVG examples, the right-scale parameter is generally larger than the left-scale parameter whereas here a range of behaviour is

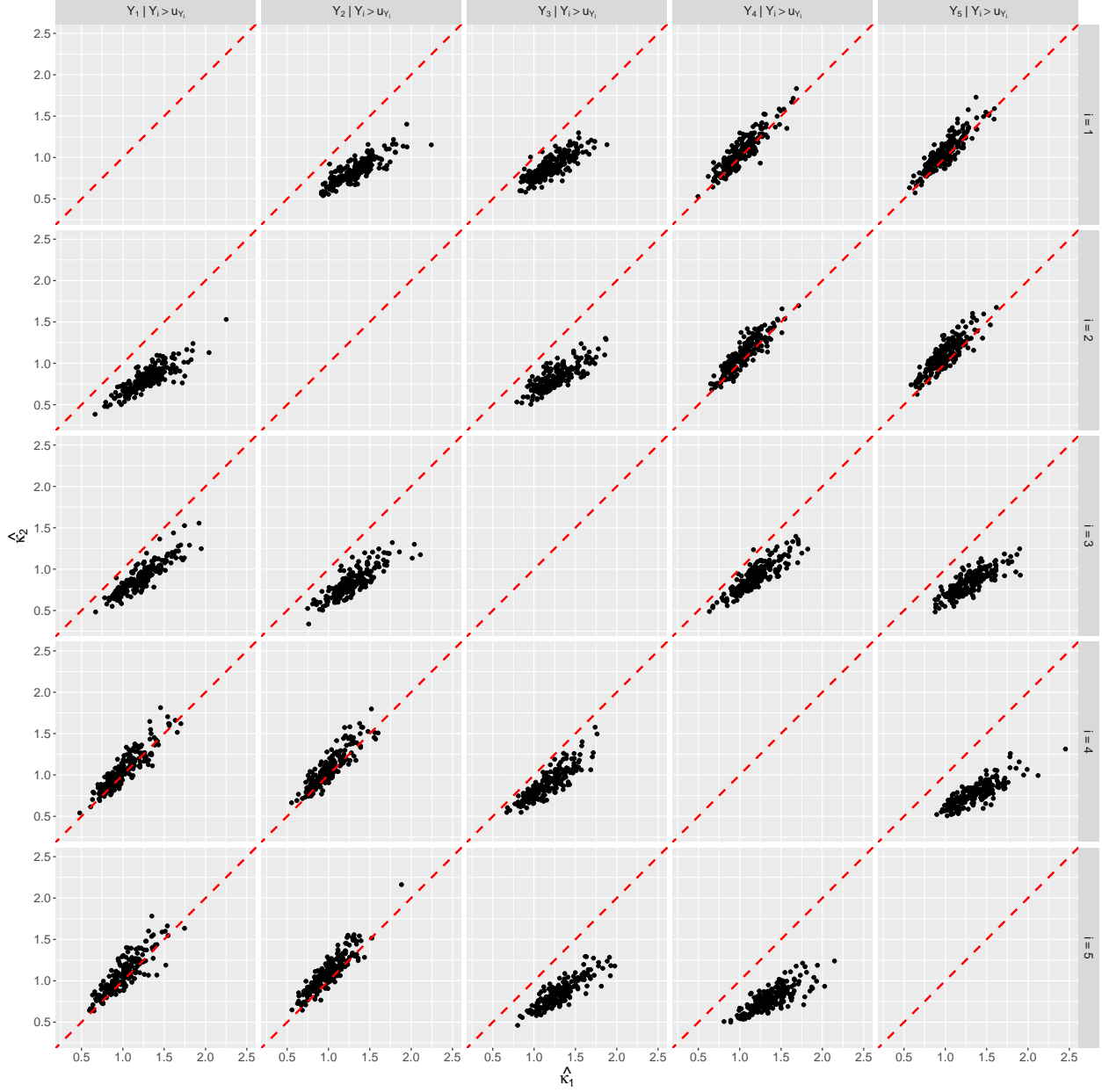


Figure S10: Scatter plots comparing $\hat{\kappa}_{1|j|i}$ and $\hat{\kappa}_{2|j|i}$ from the three-step SCMEVM with graphical covariance structure for distinct $i, j \in V$. Red dashed lines show $y = x$.

observed. This further justifies the need for a flexible, asymmetric residual distribution.

Figure S11 (left panel) shows the bias in the conditional cumulative distribution curves for $X_j | X_5 > u_{X_5}$ for the EHM and the three-step SCMEVM with graphical covariance structure. The three-step SCMEVM shows no bias but the EHM underestimates the curve over the entire range. Again, this is not surprising, as the assumption of AD is not satisfied by the data. Figure S11 (right panel) considers the bias in $\mathbb{P}[X_{|5} < u_{X_{|5}} | X_5 > u_{X_5}]$. The

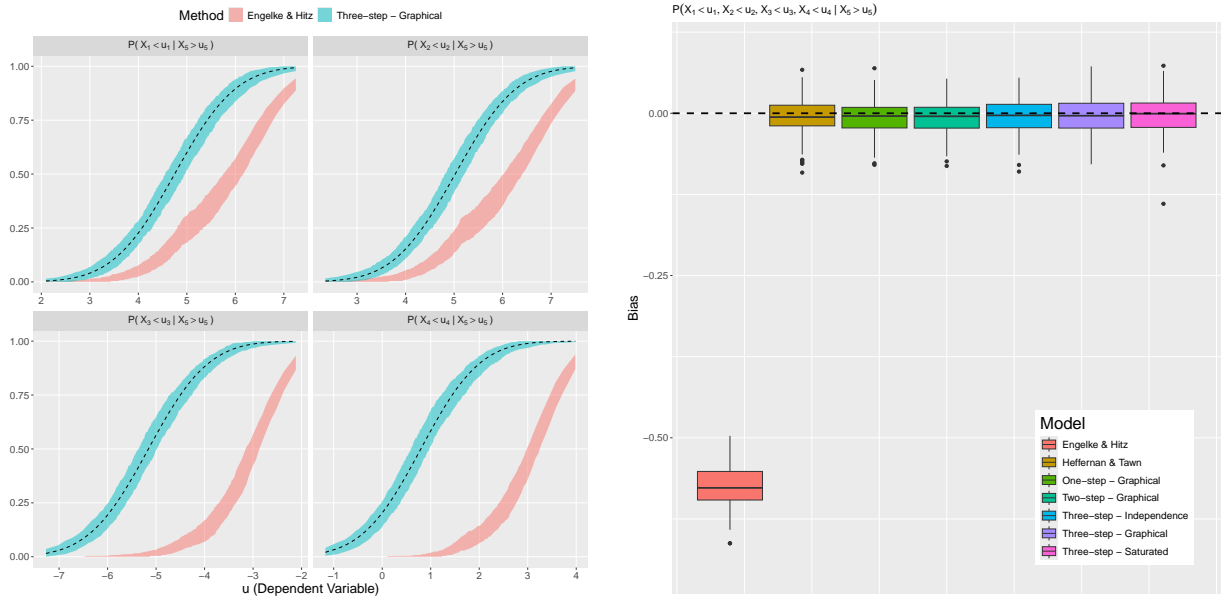


Figure S11: Polygon plots detailing 95% confidence intervals, over 200 samples, of $\mathbb{P}[X_j < u_{X_j} | X_5 > u_{X_5}]$ for $j \in V_{|5}$, when X follows a MVG distribution with negative associations (left). The estimated curves from the EHM and the three-step SCMEVM with a graphical covariance structure are in pink and blue, respectively. The true conditional cumulative distribution curves are indicated by the black dashed lines. Boxplots of the bias in $\mathbb{P}[X_{|5} < u_{X_{|5}} | X_5 > u_{X_5}]$ (right). The bias from the various models is denoted by the fill of the boxplots. The $y = 0$ line is indicated by the black dashed line.

EHM exhibits negative bias, while the CMEVM and SCMEVMs are unbiased. Finally, as in the previous studies, the SCMEVMs with graphical covariance structures are the least biased and variable, minimising the MAE and RMSE 76% and 87% of the time, respectively.

S.3.2 Multivariate Laplace Distribution

In this study, X follows a MVL distribution with mean vector $\boldsymbol{\mu}$, where μ_j are independently sampled from a uniform distribution on $(-5, 5)$, and precision matrix consistent with \mathcal{G} in Section S.2.

S.3.2.1 Weak Positive Dependence

In this simulation, associations between components are weakly positive i.e., the elements of the true correlation matrix are strictly positive but less than 0.37. We set the dependence threshold u_{Y_i} to be the 0.95-quantile of the standard Laplace distribution, resulting in approximately 250 excesses per conditioning variable. For prediction, u_{X_i} is set to the 0.95-quantile from a single sample of 10^6 from the true distribution. Figure S12 shows empirical



Figure S12: Boxplots of empirical and model-based estimates of $\Gamma_{|i}$, for each $i \in V$, when the data is generated from a MVL distribution with weak positive associations. Each row corresponds to the conditioning variable i and each column corresponds to the correlation parameter. The different models are distinguished by the colour of the boxplots. Black dashed lines show $y = 0$.

and model-based estimates of the conditional precision matrix $\Gamma_{|i}$. The estimated structure of the conditional precision matrix from both the graphical and the saturated SCMEVM is consistent with the empirical version. Analysis of other parameter estimates have been omitted, but they are very similar across all three stepwise procedures. The only point to note is that estimates for the left- and right-scale parameters in the MVAGG are very similar, raising the question of whether the generalised Gaussian would be a better choice of marginal residual distribution. However, other examples do have very different scale parameters (see Figures S6 and S10) and the more flexible asymmetric generalised Gaussian distribution is therefore recommended.

To compare predictive performance, Figure S13 (left panel) shows the bias in the conditional survival curves of $X_j | X_3 > u_{X_3}$ for $j \in V_3$. Similar to the MVG examples, the SCMEVM with graphical covariance structure is unbiased for all curves, whereas the EHM has positive bias for low values of u_{X_j} which decreases as u_{X_j} increases. Figure S13 (right panel) shows

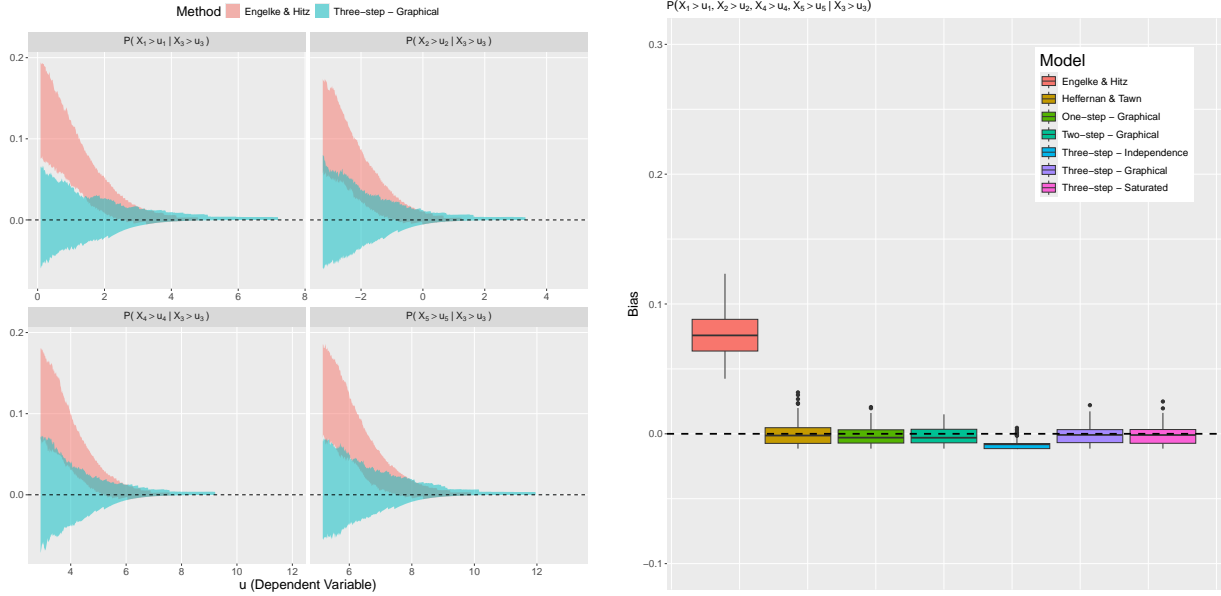


Figure S13: Polygon plots detailing 95% confidence intervals, over 200 samples, of the bias in $\mathbb{P}[X_j > u_{X_j} \mid X_3 > u_{X_3}]$ for $j \in V_{|1}$, where X follows a MVL distribution with weak positive associations (left). The bias from the EHM and the three-step SCMEVM assuming a graphical covariance structure for the residuals are in pink and blue, respectively. Boxplots of the bias in $\mathbb{P}[X_{|3} > u_{X_{|3}} \mid X_3 > u_{X_3}]$ (right). The bias from the various models is denoted by the fill of the boxplots. Black dashed lines show $y = 0$.

the bias in $\mathbb{P}[X_{|3} > u_{|3} \mid X_3 > u_{X_3}]$. The CMEVM and the SCMEVMs with graphical or saturated covariance structures are unbiased, whereas, the EHM has positive bias. Again, the three-step SCMEVM with independent residuals has negative bias because not all components of $X_{|3}$ are independent given X_3 . Similar findings are made when assessing other conditional probabilities of the form $\mathbb{P}[X_A > u_A \mid X_i > u_i]$ for all $A \subseteq V_i$ and $i \in V$. Lastly, the SCMEVMs with graphical covariance have the least amount of bias and variability, minimising the MAE and RMSE for 86% and 77% of the 75 conditional probabilities, respectively.

S.3.2.2 Strong Positive Dependence

We repeat the simulation study in Section S.3.2.1 with strong positive association between the components i.e., the entries of the true correlation matrix are all greater than 0.69. The dependence threshold u_{Y_i} is set to the 0.9-quantile for the standard Laplace distribution, for each $i \in V$. For prediction, we set u_{X_i} to the 0.95-quantile from a dataset of size 10^6 simulated from the true distribution. We omit parameter estimates since the only point to note is that a comparison of the estimates from the one-, two-, and three-step SCMEVMs shows that the dependence parameters are slightly larger for the one-step method, while the location

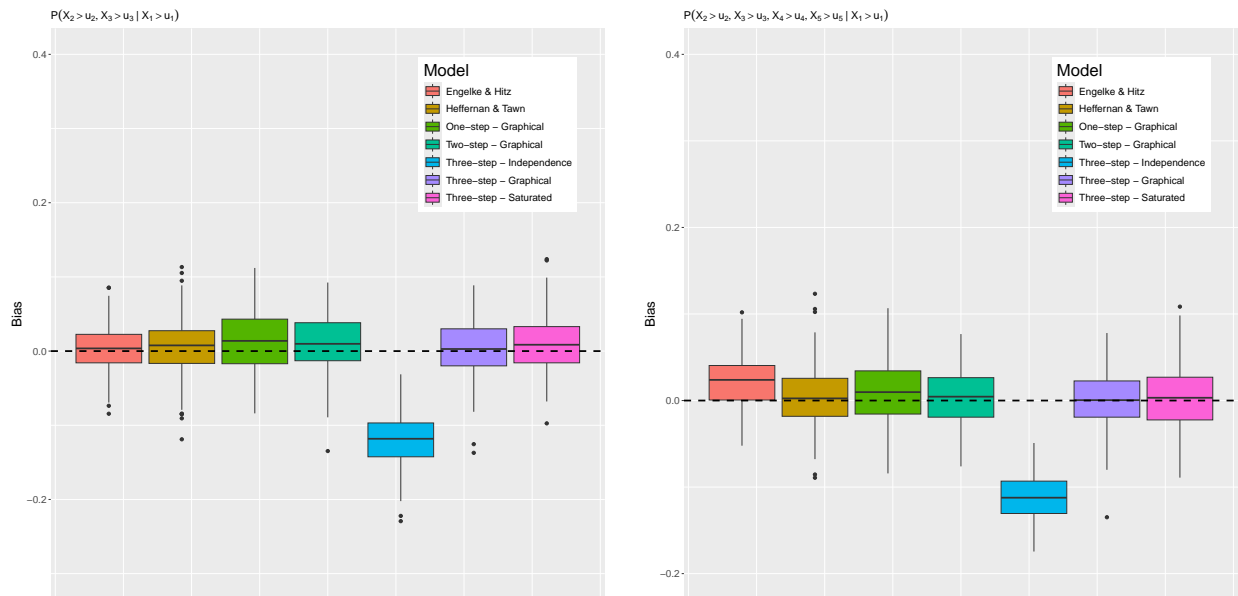


Figure S14: Boxplots of the bias in $p_1 = \mathbb{P}[X_2 > u_{X_2}, X_3 > u_{X_3} \mid X_1 > u_{X_1}]$ (left) and $p_2 = \mathbb{P}[X_{|1} > u_{X_{|1}} \mid X_1 > u_{X_1}]$ (right) when X follows a MVL distribution with strong positive associations. The bias from the various models is denoted by the fill of the boxplots. Black dashed lines show $y = 0$.

and scale parameters are slightly lower.

Figure S14 shows the bias in two tail probabilities, $p_1 = \mathbb{P}[X_2 > u_{X_2}, X_3 > u_{X_3} \mid X_1 > u_{X_1}]$ and $p_2 = \mathbb{P}[X_{|1} > u_{X_{|1}} \mid X_1 > u_{X_1}]$. In this case the EHM performs more similarly to the CMEVM and SCMEVMs. However, while it is unbiased for p_1 , it does have small positive bias for p_2 . Further, the EHM minimises the MAE and RMSE for 37 and 42, respectively, of the 75 conditional probabilities, while the three-step SCMEVM with graphical covariance structure minimises the MAE and RMSE 31 and 25 times, respectively. The CMEVM and SCMEVMs with graphical or saturated covariance structures are unbiased for both probabilities in Figure S14 though suggesting these models scale better with dimension compared to the EHM.

S.3.2.3 Negative Dependence

Finally, we consider negative associations between components. The true correlation matrix is provided in equation (S.2). The dependence threshold u_{Y_i} is set to the 0.8-quantile for the standard Laplace distribution. For prediction, we set u_{X_i} to the 0.9-quantile from a dataset

of size 10^6 simulated from the true distribution.

$$\Sigma = \begin{bmatrix} 1.000 & -0.200 & -0.139 & 0.026 & 0.022 \\ -0.200 & 1.000 & -0.243 & 0.045 & 0.038 \\ -0.139 & -0.243 & 1.000 & -0.185 & -0.158 \\ 0.026 & 0.045 & -0.185 & 1.000 & -0.276 \\ 0.022 & 0.038 & -0.158 & -0.276 & 1.000 \end{bmatrix} \quad (\text{S.2})$$

The only point to note on the parameter estimates is that $\beta_{j|i}$ tends to always be slightly higher for the one-step SCMEVM than for the two- and three-step SCMEVMs. Figure S15 (left panel) shows 95% confidence intervals for the conditional cumulative distribution curves of $X_j \mid X_4 > u_{X_4}$ for $j \in V_4$ and for the EHM and the three-step SCMEVM with graphical covariance structure. As with the MVG distribution with negative association, the SCMEVM captures the curves perfectly while the EHM underestimates all curves. The SCMEVMs with graphical covariance structure minimise the MAE and RMSE 63% and 59% of the time, respectively. The three-step SCMEVM with saturated covariance structure also performs very well minimising the metrics 23% and 28% of the time, respectively. However, the numerical values of the metrics are almost indistinguishable for the two models as shown in Figure S15 (right panel) where we plot the bias in $\mathbb{P}[X_{j_4} < u_{X_{j_4}} \mid X_4 > u_{X_4}]$. The EHM and SCMEVM with independent residuals are both biased, while the SCMEVMs with graphical or saturated covariance structure are unbiased. The CMEVM predictions exhibit a small positive bias, although the reason for this is unclear.

S.3.3 Multivariate t -distribution

For this study, X has a MVT distribution with mean $\boldsymbol{\mu} = \mathbf{0}$, $k = 5$ degrees of freedom, and a dispersion matrix with inverse consistent with \mathcal{G} in Section S.2.1. We consider weak positive, strong positive, and negative associations in X in Sections S.3.3.1, S.3.3.2, and S.3.1.3, respectively. For all simulations, the dependence threshold u_{Y_i} is set to the 0.8-quantile from the standard Laplace distribution, resulting in approximately 1,000 excesses per conditioning variable. As with the previous examples, parameter estimates are omitted unless of specific interest.

S.3.3.1 Weak Positive Dependence

In this simulation, we ensure the associations between components are weakly positive i.e., entries in the dispersion matrix are strictly positive but less than 0.17. For prediction, we set $u_{X_i} = 0.75$ for each $i \in V$.

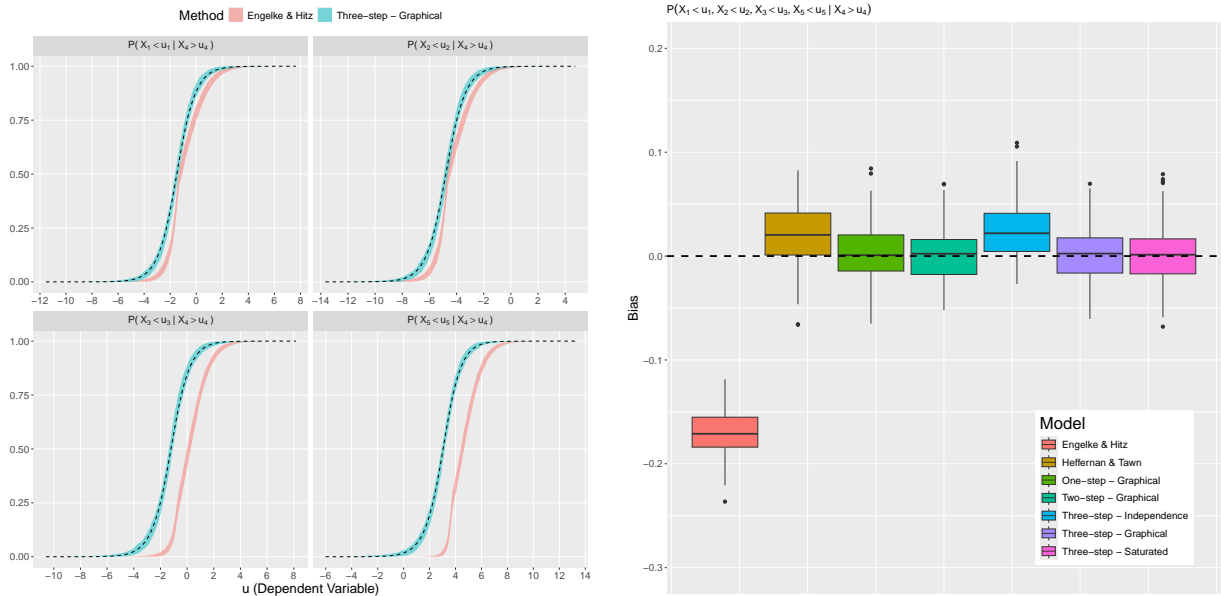


Figure S15: Polygon plots detailing 95% confidence intervals, over 200 samples, of the bias in $\mathbb{P}[X_j < u_{X_j} \mid X_4 > u_{X_4}]$ for $j \in V_4$, where X follows a MVL distribution with negative associations (left). The bias from the EHM and the three-step SCMEVM assuming a graphical covariance structure for the residuals are in pink and blue, respectively. The true conditional cumulative distribution curves are given by the black dashed lines. Boxplots of the bias in $\mathbb{P}[X_{|4} < u_{X_{|4}} \mid X_4 > u_{X_4}]$ (right). The bias from the various models is denoted by the fill of the boxplots. The $y = 0$ line is given by the black dashed line.

Figure S16 shows empirical and model-based estimates of the conditional precision matrix $\Gamma_{|i}$. The estimated structure of the conditional precision matrix from both the graphical and saturated SCMEVMs is again consistent with the empirical version. Analysis of other parameter estimates has been omitted, other than noting that estimates of $\beta_{j|i}$ from the one-step SCMVEM are generally larger than corresponding estimates from the two- and three-step SCMEVMs.

Figure S17 (left panel) shows the bias in the conditional survival curves of $X_j \mid X_3 > u_{X_3}$ for $j \in V_3$. Similar to the MVG and MVL examples, the SCMVEM with graphical covariance structure is unbiased for all curves, whereas, the EHM exhibits positive bias for low values of u_{X_j} which decreases as u_{X_j} increases. We have also included the estimated curve from the CMEVM to show there is little difference between the estimates from the CMEVM and the SCMEVM with graphical covariance structure.

Figure S17 (right panel) shows the bias in $\mathbb{P}[X_{|3} > u_{|3} \mid X_3 > u_{X_3}]$. As expected, the CMEVM estimates are unbiased, the EHM exhibits positive bias, and the three-step SCMEVM with independent residuals exhibits negative bias because not all the components of $X_{|3}$ are in-



Figure S16: Boxplots of empirical and model-based estimates of $\Gamma_{i|}$, for each $i \in V$, when the data is generated from a MVT distribution with weak positive associations. Each row corresponds to the conditioning variable i and each column corresponds to the correlation parameter. The colour of the boxplots distinguishes the different models. Black dashed lines show $y = 0$.

dependent given X_3 . Interestingly, the fully parametric SCMEVMs with graphical or saturated covariance structures exhibit a very small negative bias. Despite this, the three-step SCMEVM with graphical structure is the least biased and variable model as it minimises the MAE and RMSE for 38 and 46, respectively, of the 75 conditional tail probabilities across all models. In comparison, the CMEVM only minimises the metrics 21 and 13 times, respectively. This suggests there is little difference between the CMEVM and the SCMEVM in this scenario.

Assessing diagnostic plots from the SCMEVM creates no concern with the model fit. Therefore, to fix the slight underestimation from the SCMEVMs in Figure S17 (right panel), we may need to increase N' used in Algorithm 3.5 of the main text (we let $N' = 250,000$ in this simulation). Alternatively, we may wish to simulate data from the fitted model for $X \mid X_i > u_{X_i}$ for each $i \in V$, rather than for the more general simulation from Section 3.3 in the main text which simulates data for the entire domain with the extreme region

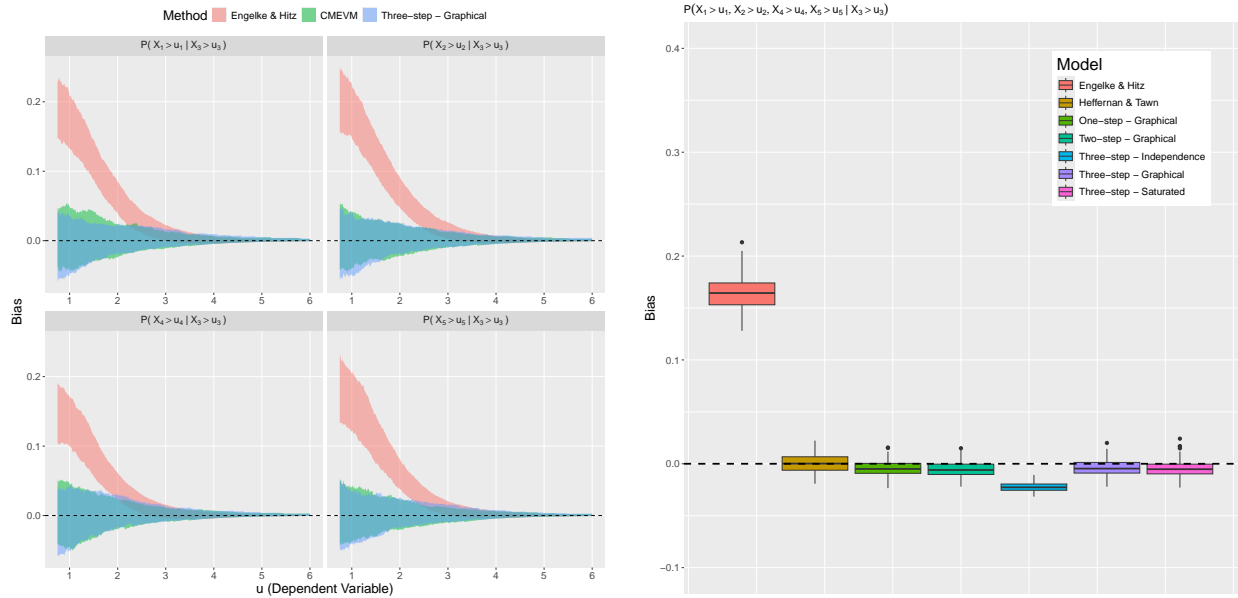


Figure S17: Polygon plots detailing 95% confidence intervals, over 200 samples, of the bias in $\mathbb{P}[X_j > u_{X_j} | X_3 > u_{X_3}]$, for each $j \in V_{|1}$, where X follows a MVT distribution with weak positive associations (left). The bias from the EHM, the CMEVM, and the three-step SCMEVM assuming a graphical covariance structure for the residuals are in pink, green, and blue, respectively. Boxplots of the bias in $\mathbb{P}[X_{|3} > u_{X_{|3}} | X_3 > u_{X_3}]$ (right). The fill of the boxplots distinguishes the different models. Black dashed lines show $y = 0$.

corresponding to at least one component is extreme.

S.3.3.2 Strong Positive Dependence

We now allow strong positive associations between the components. The only note on the parameter estimates is that the CMEVM dependence parameters, tend to be higher for the one-step SCMEVM compared to the two- and three-stepwise SCMEVMs, while the marginal AGG parameters (excluding the shape) tend to be lower for the one-step SCMEVM. Setting $u_{X_i} = 1.25$ for each $i \in V$, Figure S18 (left panel) shows the bias in the conditional survivor curves of $X_j | X_2 > u_{X_2}$ for $j \in V_{|2}$, and for the EHM and the three-step SCMEVM with graphical covariance structure. The EHM is biased for low values of u_{X_j} but this diminishes as u_{X_j} increases. In contrast, the three-step SCMEVM with a graphical covariance structure is unbiased across all curves. Figure S18 (right panel) shows the bias in $\mathbb{P}[X_{|3} > u_{X_{|3}} | X_3 > u_{X_3}]$. The EHM has positive bias, while the CMEVM and the stepwise SCMEVMs with graphical or saturated covariance structures are unbiased. Once again, the SCMEVMs with graphical covariance structure are the least biased and the least variable, minimising both the MAE and RMSE for 48 of the 75 conditional tail probabilities.

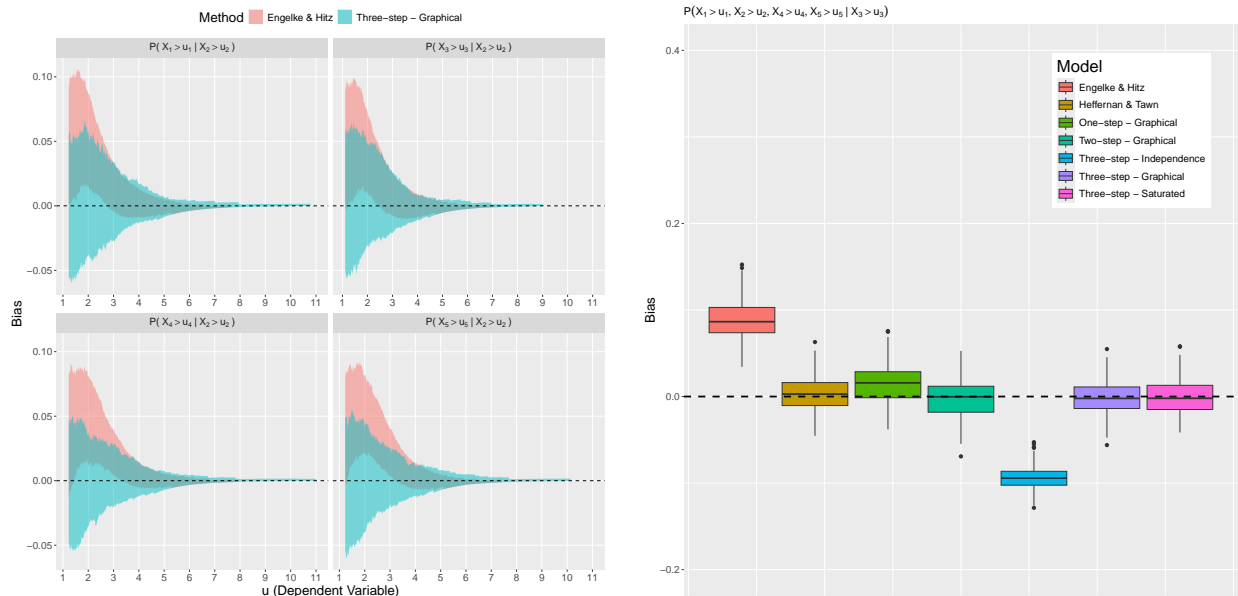


Figure S18: Polygon plots detailing 95% confidence intervals, over 200 samples, of the bias in $\mathbb{P}[X_j > u_{X_j} | X_2 > u_{X_2}]$ for $j \in V_{|2}$, where X follows a MVT distribution with strong positive associations (left). The bias from the EHM and the three-step SCMEVM assuming a graphical covariance structure for the residuals are in pink and blue, respectively. Boxplots of the bias in $\mathbb{P}[X_{|3} > u_{X_{|3}} | X_3 > u_{X_3}]$ (right). The bias from the various models is denoted by the fill of the boxplots. Black dashed lines show $y = 0$.

S.3.3.3 Negative Dependence

Finally, we allow for weak negative associations between the components. For prediction, we set u_{X_i} to the 0.9-quantile from a dataset of size 10^6 simulated from the true distribution. Figure S19 (left panel) shows 95% confidence intervals for the conditional cumulative distribution curves of $X_j | X_3 > u_{X_3}$ for $j \in V_{|3}$ and for the EHM and the three-step SCMEVM with graphical covariance structure. As with the MVG and MVL distributions with negative associations, the three-step SCMEVM captures all curves perfectly, whereas the EHM always underestimates. Figure S19 (right panel) shows the bias in $\mathbb{P}[X_{|5} < u_{X_{|5}} | X_5 > u_{X_5}]$. The EHM performs poorly due to its inability to capture the negative dependence, while predictions from the CMEVM and the SCMEVMs with graphical or saturated covariance structures are unbiased. The SCMEVMs with a graphical covariance structure minimise the MAE and RMSE metrics for 79% and 72%, respectively, of conditional tail probabilities.

S.3.4 Multivariate Pareto Distribution

To test the SCMEVM under AD, we repeat the simulation study for X with a MVP distribution such that the parameter matrix is consistent with \mathcal{G} in Section S.2. For the CMEVM,

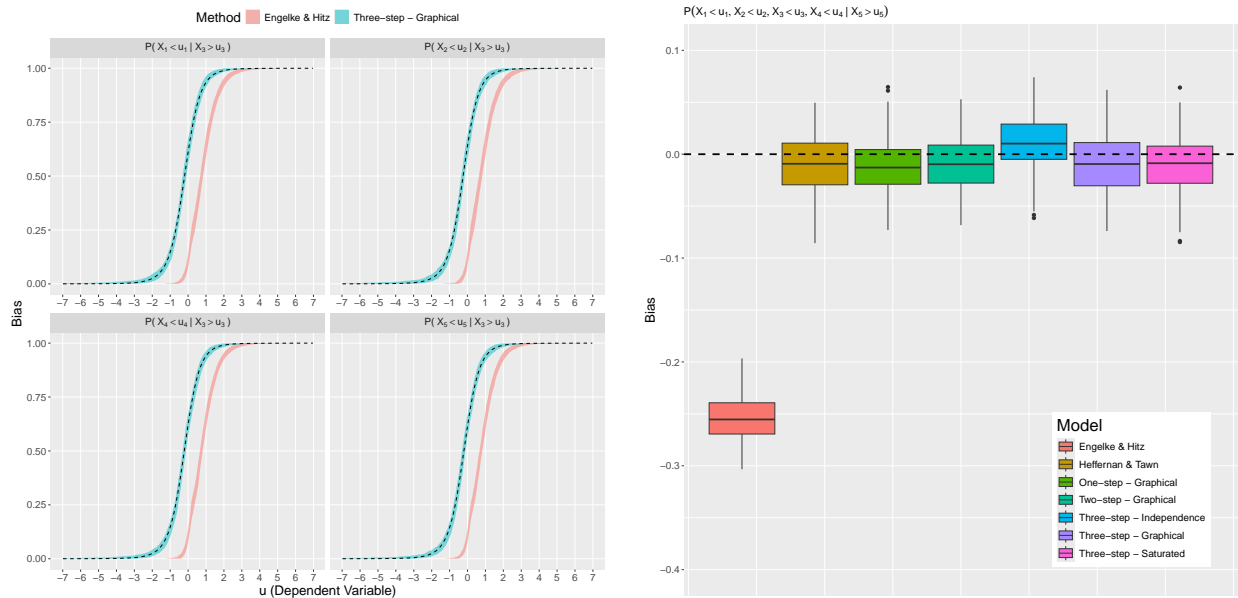


Figure S19: Polygon plots detailing 95% confidence intervals, over 200 samples, of the bias in $\mathbb{P}[X_j < u_{X_j} | X_3 > u_{X_3}]$ for $j \in V_3$, where X follows a MVT distribution with negative associations (left). The bias from the EHM and the three-step SCMEVM assuming a graphical covariance structure for the residuals are in pink and blue, respectively. The true conditional cumulative distribution curves are given by the black dashed lines. Boxplots of the bias in $\mathbb{P}[X_{|5} < u_{X_{|5}} | X_5 > u_{X_5}]$ (right). The bias from the various models is denoted by the fill of the boxplots. The $y = 0$ line is given by the black dashed line.

we use only data above the dependence threshold u_{Y_i} set at the 0.90-quantile of the standard Laplace distribution. The EHM uses all data since, by construction, the data is on standard Pareto margins. For prediction, $u_{X_i} = 11$ for each $i \in V$.

Figure S20 shows empirical and SCMEVM model-based estimates of $\Gamma_{|i}$ and transformed model-based estimates from the EHM. Again, the empirical structure is retained in all models. The EHM and SCMEVMs have a very close correspondence, although the former has less variability due to the larger sample size. Figure S21 (left panel) shows the bias in the conditional survivor curves for $X_j | X_5 > u_{X_5}$, $j \in V_{|5}$. Both the EHM and the three-step SCMEVM with graphical covariance are unbiased, but estimates from the former are slightly less variable due to the larger sample size. Figure S21 (right panel) shows the bias in $\mathbb{P}[X_{|5} > u_{X_{|5}} | X_5 > u_{X_5}]$. As expected, the EHM is unbiased while the SCMEVMs exhibit a slight negative bias perhaps due to the α parameter not converging to the true value, $\alpha = 1$, that lies on the edge of the parameter space. However, the bias in the SCMEVMs with graphical and saturated covariances is small. Considering all 75 conditional tail probabilities, the EHM minimises both the MAE and RMSE metrics the majority of the time. Excluding the EHM, which is the only model specifically designed for AD data, the SCMEVMs with



Figure S20: Boxplots of empirical and model-based estimates of $\Gamma_{|i}$, for each $i \in V$, when the data is generated from a MVP distribution. Each row corresponds to the conditioning variable i and each column corresponds to the correlation parameter. The various models are denoted by the colour of the boxplots. Black dashed lines show $y = 0$.

graphical covariance minimise the metrics 83% and 89% of the time, respectively, suggesting that the SCMEVM is an acceptable alternative to the EHM when the extremal dependence class cannot be pre-determined.

S.4 Additional figures for Section 5

We obtain 200 non-parametric bootstrap samples of the declustered river discharge data from the upper Daube River basin. For each bootstrapped dataset, we fit (i) the EHM, (ii) the three-step SCMEVM with graphical covariance structure, (iii) the three-step SCMEVM with saturated covariance structure, and (iv) the three-step SCMEVM with graphical covariance structure. The graph for (i) and (ii) is given by the undirected tree induced by the flow connections of the upper Danube River basin (Figure 1 (left panel) of the main text) while the graph for (iv) is inferred (Figure 6 (right panel) of the main text).

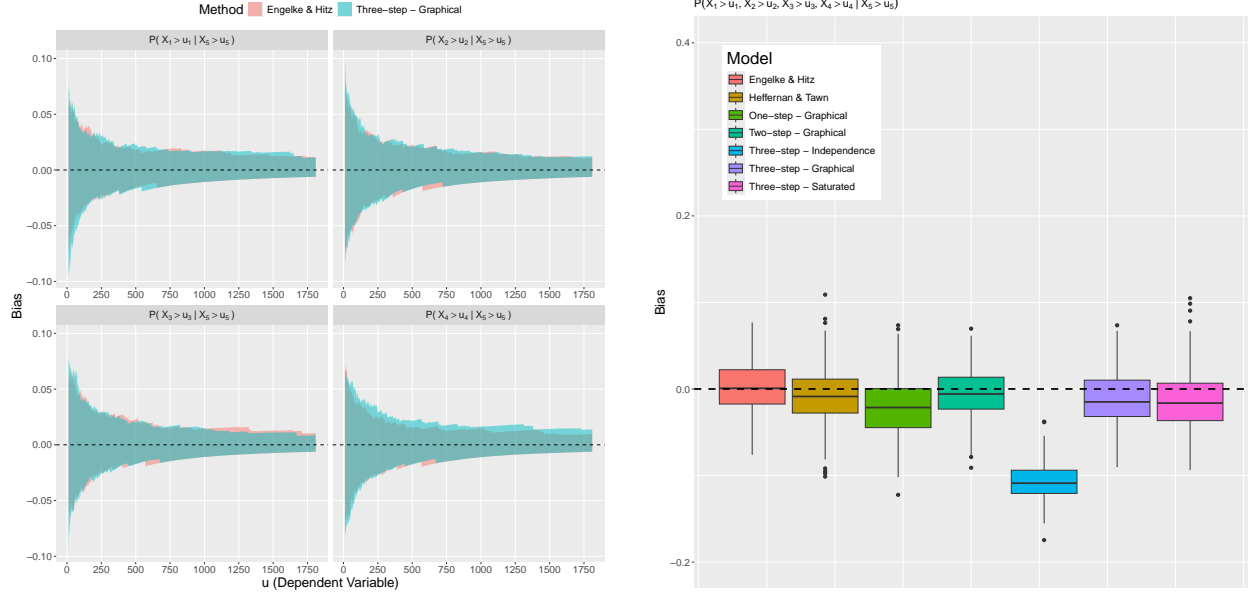


Figure S21: Polygon plots detailing 95% confidence intervals, over 200 samples, of the bias in $\mathbb{P}[X_j > u_{X_j} | X_1 > u_{X_1}]$ for $j \in V_{|1}$, where X follows a MVP distribution (left). The bias from the EHM and the three-step SCMEVM assuming a graphical covariance structure for the residuals are in pink and blue, respectively. Boxplots of the bias in $\mathbb{P}[X_{|5} > u_{X_{|5}} | X_5 > u_{X_5}]$ (right). The bias from the various models are denoted by the fill of the boxplots. Black dashed lines show $y = 0$.

For each of the fitted models and for each bootstrapped dataset, we obtain a single simulation which is used for prediction. Empirical and model-based estimated for $\chi_{i,j}(u)$ are obtained for $i, j \in V$, $i > j$, and $u \in \{0.8, 0.85, 0.9\}$, where $V = \{1, \dots, 31\}$. The point estimates in Figure S22 are the median estimates over the two sets of estimates for $\chi_{i,j}(u)$. As in Figure 7 of the main text, the SCMEVMs better capture the extremal dependence structure than the EHM. Figure S23 shows a similar comparison but for $\chi_A(u)$ where $A \subset V$ are 500 randomly sampled triplets, and $u \in \{0.8, 0.85, 0.9\}$. Again, the SCMEVMs better capture the extremal dependence in the upper Danube River basin. Although for higher thresholds the EHM is less biased for moderately dependent triplets, the bias for low dependent triplets increases as the threshold increases. Similar conclusions can be made for (iv), however, the magnitude of the bias is much smaller. Model (iv) appears to perform better than (ii) and rectifies the systemic underestimation in (iii). Thus, (iv) appears to have best predictive performance across multiple components.

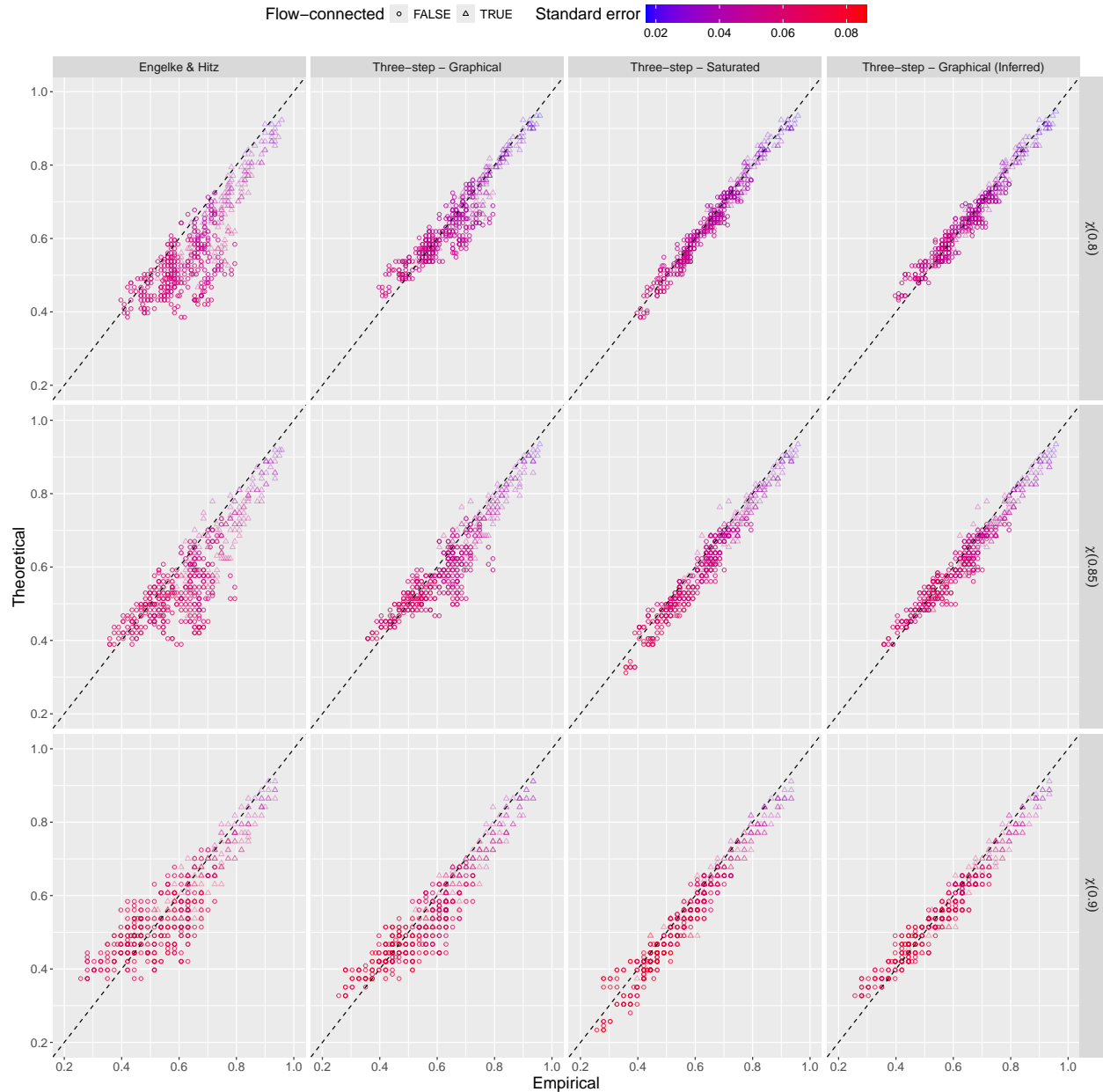


Figure S22: Empirical and model-based estimates of $\chi_{i,j}(u)$ for $u \in \{0.8, 0.85, 0.9\}$ (top to bottom), and $i, j \in V$ but $i > j$. Model-based estimates use the EHM (left) and the three-step SCMEVM with graphical covariance (centre left), with structure given in Figure 1 (left panel) of the main text, the three-step SCMEVM with saturated covariance (centre right) and graphical covariance (right) with structure given in Figure 6 (right panel) of the main text. Black dashed lines show $y = x$. Circles (triangles) show flow-connected (flow-unconnected). The colour shows the standard error of the model-based estimates.

Supplementary References

Engelke, S. and Hitz, A. S. (2020). Graphical models for extremes. *Journal of the Royal Statistical Society: Series B (Statistical Methodology)*, 82(4):871–932.

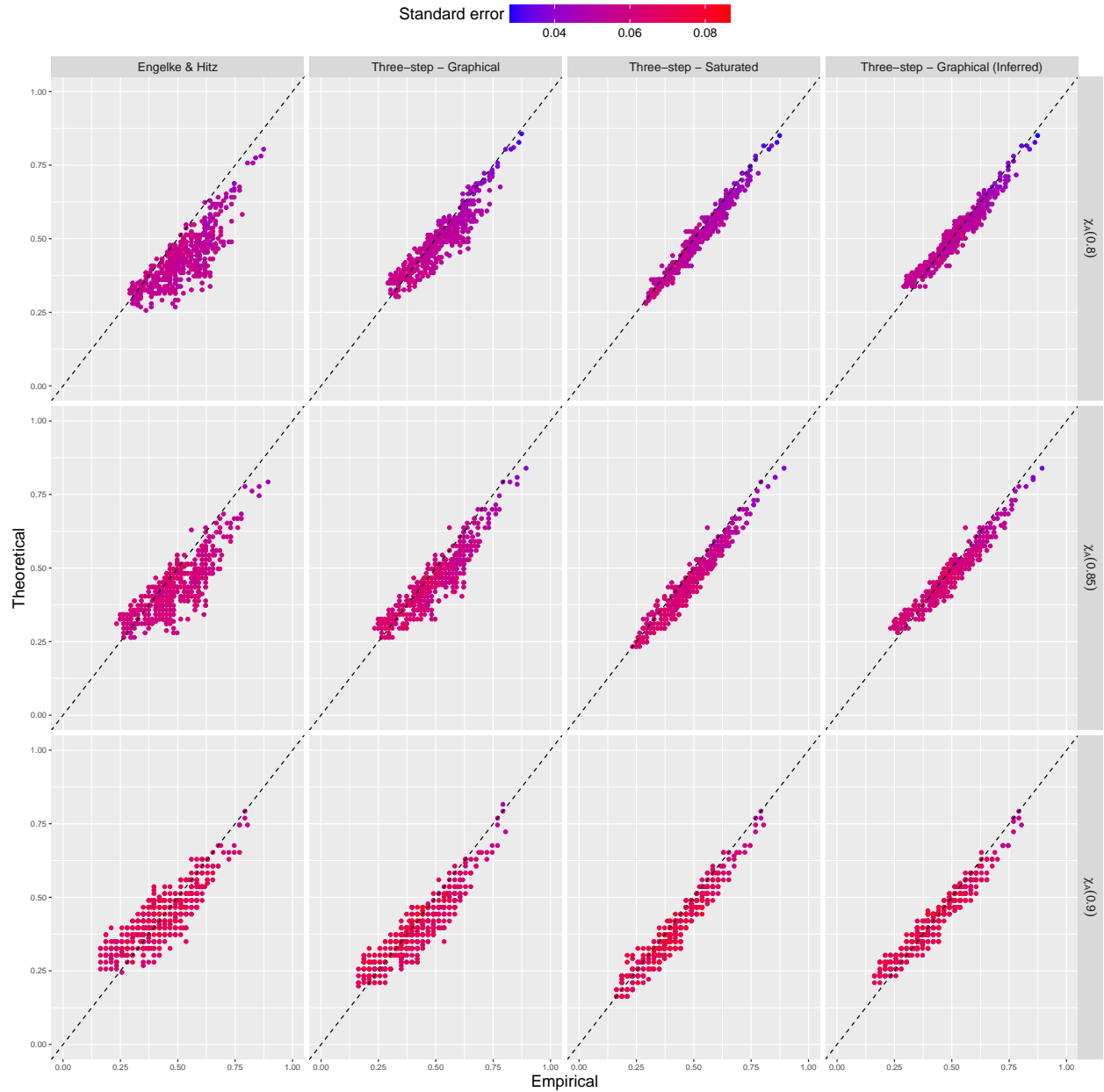


Figure S23: Empirical and model-based estimates of $\chi_A(u)$ for $u \in \{0.8, 0.85, 0.9\}$ (top to bottom) for 500 randomly selected triplets of $A \subset V$. Model-based estimates use the EHM (left) and the three-step SCMEVM with graphical covariance (centre left), with structure given in Figure 1 (left panel) of the main text, the three-step SCMEVM with saturated covariance (centre right) and graphical covariance (right) with structure given in Figure 6 (right panel) of the main text. Black dashed lines show $y = x$. The colour shows the standard error of the model-based estimates.

Heffernan, J. E. and Tawn, J. A. (2004). A conditional approach for multivariate extreme values (with discussion). *Journal of the Royal Statistical Society: Series B (Statistical Methodology)*, 66(3):497–546.

- Nagler, T. and Czado, C. (2016). Evading the curse of dimensionality in nonparametric density estimation with simplified vine copulas. *Journal of Multivariate Analysis*, 151:69–89.
- Wadsworth, J. and Tawn, J. (2022). Higher-dimensional spatial extremes via single-site conditioning. *Spatial Statistics*, 51:100677.